UNIVERSITY OF MILANO-BICOCCA

Department of Earth and Environmental Sciences

PhD Course in Earth Sciences (XXVII cycle)

Academic Year 2014

Brittle deformation in phyllosilicate-rich mylonites: implication for failure modes, mechanical anisotropy, and fault weakness

Francesca Bolognesi

Supervisor: Dott. Andrea Bistacchi

Co-supervisor: Dott. Sergio Vinciguerra

Brittle deformation in phyllosilicate-rich mylonites: implication for failure modes, mechanical anisotropy, and fault weakness

Francesca Bolognesi

Supervisor: Dott. Andrea Bistacchi

Co-supervisor: Dott. Sergio Vinciguerra

DIPARTIMENTO DI SCIENZE
DELL'AMBIENTE E DEL TERRITORIO
E DI SCIENZE DELLA TERRA

Università degli Studi di Milano-Bicocca

UNIVERSITA' DEGLI STUDI DI MILANO

BICOCCA

British
Geological Survey
NATURAL ENVIRONMENT RESEARCH COUNCIL

VT·VI TAM
HAB EANT

University of
Leicester

1 Table of contents

1. Introduction

Phyllosilicates, even in relatively small quantities, dramatically influence the mechanical behavior of rocks (e.g. Collettini et al., 2009; Van Diggelen et al., 2010; Holdsworth et al., 2011). In laboratory triaxial tests on foliated rocks, for a content in phyllosilicates greater than 20-25%, a relevant mechanical anisotropy appears, as the internal friction coefficient (tangential stress/normal stress at failure) varies between 0.3 and 0.7 with orientation of the sample with respect to the maximum compressive stress (Jaeger et al. 2007, Kronenberg et al. 1990; Moore & Lockner 2004, Bistacchi et al.2012). This reflects different fracture modes: when the foliation is favorably oriented, fractures develop along it and the rocks are weak, whilst when fractures cut the foliation at a high angle, rocks are stronger (Jaeger et al., 2007).

This kind of mechanical anisotropy is one possible explanation for the relative and absolute fault weakness shown by non-Andersonian misoriented faults (i.e. faults with an orientation, with respect to the regional stress field, not fulfilling Anderson's theory of faulting; Anderson, 1951; Sibson, 1985). Examples of misoriented faults are low angle normal faults (LANFs, Wernicke 1982), high angle reverse faults (Cox 1995; Butler et al. 2008) and strike slip faults developed at a high angle with the most compressive regional stress axis (Townend and Zoback, 2004).

In this thesis I have considered two field examples of misoriented faults represented by the Simplon Line Fault Zone (SFZ), in the Swiss Alps, and a zone of (ultra)cataclastic bands in the Grandes Rousses Massif of the French Alps (GRM). These structures have been characterized from the regional scale (paleostress), to the meso-scale (fault zone architecture), and micro-scale (optical microscope, SEM and micro-CT). Moreover, I have characterized the petrophysical properties and mechanical anisotropy of the GRM rocks with density, porosity, uniaxial (UCS) and triaxial (TXT) lab tests performed at the Environmental Science Centre of the British Geological Survey in Keyworth (Nottingham,UK).

2. Weakening mechanisms and mechanical anisotropy evolution in phyllosilicate-rich cataclasites developed after mylonites in a low-angle normal fault (Simplon Line, Western Alps)

Francesca Bolognesi and Andrea Bistacchi

Department of Earth and Environmental Sciences, Università degli Studi di Milano Bicocca, Italy

1.1 Abstract

The Simplon Fault Zone is a late-collisional low-angle normal fault of the Western Alps. The fault activity lead to differential exhumation of the hanging wall and footwall. During the fault activity the hanging wall is characterized by brittle deformation only. On the other hand, the footwall is characterized by a 1 km thick shear zone (the Simplon Fault Zone), which continuously evolved, during exhumation, from amphibolite facies conditions to brittle-cataclastic deformations. Due to progressive localization of the active section of the shear zone, this evolution results in a layered structure, with higher temperature fault rocks preserved at the periphery of the shear zone, and cataclasites occurring at the core (indicated as the Simplon Line). The nucleation of cataclasites, which develop after greenschist facies mylonites, have been studied at the periphery of the cataclasite zone. It is characterized by fractures, micro-faults and ultracataclasite seams that develop along the mylonitic S/C/C' fabric, exploiting the weak phases mainly represented by muscovite and chlorite. Approaching the proper fault core, both the thickness and frequency of cataclasite horizons increase, and, as their thickness increases, they become less and less foliated. The fault core itself is exposed only in a few outcrops. In some cases it is simply represented by thicker cataclasite horizon. In other cases, these cataclasites have been dissected by a network of calcite veins, possibly related to carbonate lenses that have been dragged along the fault zone, and probably indicating episodic events of anomalously high fluid pressure. In conclusion, weakening mechanisms that may be considered for the Simplon Line include (1) the exploitation of the mechanical and textural anisotropy, represented by the S/C/C' mylonitic foliation, and (2) some later, and probably episodic, events of elevated fluid pressure, evidenced by calcite veins at the fault core.

1.2 Introduction

The Simplon Fault Zone is a late-collisional low-angle normal fault (LANF) of the Western Alps. As for other LANFs, its peculiarity is represented by the anomalous orientation of the fault surface with respect to the regional stress field and by the development of brittle deformation by exploiting the pre-existing phyllosilicate-rich mylonitic fabric.

LANFs show a dip angle < 30° and are quite common in nature in different tectonic settings in the continental crust, particularly in rift systems (e.g. Morley 1999, Cowan et al. 2003, Dean et al., 2008, Lecomte et al., 2011, 2010), metamorphic core complexes (e.g. Wernicke, 1981, Lister & Davis 1989, Forster & Lister 1999) or, as in Simplon case, in extensional post-collisional settings (Mancktelow, 1985; Massironi et al., 2011, Collettini & Barchi 2004; Smith et al. 2007).

In large-scale LANFs, which crosscut a several-km thick section of the continental crust, deformation in the footwall, which experiences a relevant exhumation, evolves from higher temperature "ductile" crystal-plastic mechanisms to lower temperature brittle frictional mechanisms, as evidenced in the Sibson (1977) and Scholz (2002) fault zone model. This evolution is commonly recorded and preserved in a zoned ductile-to-brittle shear zone (up to 3 km thick) in the upper footwall (Wernicke 1981), reflecting the localization of deformation during exhumation. From bottom to top, this is typically composed by (e.g. Wernicke, 1981): (1) foliated and lineated mylonites formed in dominantly simple shear by plastic or semibrittle, pressure insensitive mechanisms; (2) a thinner zone of protocataclasites/ breccias (commonly chlorite-epidote rich) formed in a cataclastic flow regime; and (3) a thin (0–3 m) zone of fine-grained ultracataclasites or "microbreccias" with a sharp, striated detachment fault surface at its top. Due to differential exumation the hangingwall is generally much less deformed than the footwall.

LANFs are a typical example of relatively weak faults, since they are not optimally oriented if compared to the Andersonian fault model (Anderson, 1905; Sibson, 1985), and hence imply a weakling mechanism to explain their activity. Different mechanisms have been proposed to promote slip along misoriented fault zones: (1) mechanisms involving layers of particularly weak fault gouge, containing minerals with extremely low friction coefficients (e.g. Moore and

Rymer, 2007; C. Collettini et al., 2009; Smith & Faulkner 2010); (2) mechanisms involving elevated fluid pressure (e.g.Rice, 1992, Byerlee 1990; Axen 1992; Faulkner & Rutter 2001; Collettini et al., 2006), (3) mechanisms involving a rotation of principal stress axes within the fault zone which may favour slip (e.g.Rice, 1992); and (4) finally mechanisms involving the mechanical anisotropy and weakness of foliated phyllosilicate-rich rocks (Bistacchi et al., 2012; Shea and Kronenberg, 1993).

Phyllosilicates, even in relatively small quantities, dramatically influence the mechanical behaviour of rocks (e.g. Collettini et al., 2009; Van Diggelen et al., 2010; Holdsworth et al., 2011). In laboratory triaxial tests on foliated rocks, for a content in phyllosilicates greater than 20-25%, a relevant mechanical anisotropy appears, as the internal friction coefficient (tangential stress/normal stress at failure) varies between 0.3 and 0.7 with orientation of the sample with respect to the maximum compressive stress (Bistacchi et al, 2012). This reflects different fracture modes: when the foliation is favourably oriented, fractures develop along it and the rocks are weak, whilst when fractures cut the foliation at high angle, rocks are stronger (Jaeger et al., 2007). A foliated rock characterized by a (shape and crystallographic) preferred orientation of phyllosilicates is weak due to the weakness of (001) basal planes (Kronenberg et al., 1990), and theoretical studies show that the fraction of weak minerals needed to weaken a polymineralic rock is relatively small (e.g. Handy, 1990; Rawling, 2002), particularly if the phyllosilicates are organized in continuous films, as in a lepidoblastic texture (e.g. Bistacchi et al., 2012).

In this contribution we investigate the different failure modes of phyllosilicate-rich mylonites deformed under brittle conditions (producing very fine-grained cataclasites) along the Simplon Line (SL), which develops in mylonitic rocks of the Simplon Fault Zone (SFZ; Bearth, 1956; Mancktelow, 1985). The SFZ is LANF developed in a post-collisional setting, in the metamorphic core of Alps. It shows a markedly asymmetric architecture: the footwall, which experienced an exhumation of the order of several kilometres (Campani et al., 2010a), is characterized by several hundred meters thick amphibolite to greenschist facies mylonites (Mancktelow, 1992); the hanging wall, already exhumed before the activity of the SFZ, is just characterized by brittle deformations (which overprint older metamorphic fabrics). The SL is the inner portion of the

fault zone, characterized by cataclasites related to the last stages of the SFZ's activity, and overprinting the higher-temperature mylonites (Bearth, 1956; Mancktelow, 1985; Campani et al., 2010b).

By means of meso- and micro-structural analysis, we have characterized the evolution of the weakening mechanism that were active along the SFZ and SL. We will focus particularly on (1) microstructures produced by brittle activation of a phyllosilicate-rich mylonitic foliation, (2) evidences of activity along misoriented structures, and the contemporaneous lack of nucleation/activity of Andersonian surfaces, which provides a measure of the fault zone weakness, and on (3) the progressive strain localization, which eventually allowed relatively high-pressure fluids to access the fault core, inducing a further weakening.

1.3   Structure and tectonic evolution of the SFZ

The SFZ dips at c. 25° towards the SW, and its trace develops for 30 km in Switzerland and Italy, between the Ossola and Rhone Valleys (Bearth, 1956). Some of the best outcrops are in the Simplonpass area (Figure 1). Towards the Northwest it is connected to the Rhone Line: a dextral E-W fault (Campani et al., 2010b). Towards the Southeast, it is still not unequivocally clear, mainly due to a gap in outcrops in the Ossola Valley, whether the Simplon Line merges with the E-W brittle Centovalli Line in Val Bognanco (Steck, 2008), or it if continues in the NE-SW ductile Isorno Shear Zone in the homonymous valley to the NE of Domodossola (Mancktelow, 1992).

The footwall of the SFZ corresponds to the Toce Dome, which, together with the Ticino Dome, forms the Lepontine Dome (Steck and Hunziker, 1994). The footwall is characterized by a 1-km-thick mylonitic horizon (Mancktelow, 1985, used the term SFZ just for this mylonitic belt), which evolved, due to differential exhumation, from conditions at the boundary between the amphibolite and greenschist facies, towards lower temperatures (Mancktelow, 1985; Mancktelow, 1992; Mancel and Merle, 1987; Steck, 1987; Steck, 2008; Campani et al., 2010b). The brittle detachment dividing the footwall from the hanging wall consists of a narrow zone, the SL, mapped by Bearth (1972), with cataclastic fault rocks overprinting the mylonites (Figure 1). Kinematic indicators from both ductile and brittle fault rocks of the SFZ and SL show a consistent top-down-to-SW shear sense (Mancktelow, 1985; Grosjean et al., 2004). The

footwall mylonites, and particularly the higher-temperature ones, are undulated at the mega- and macro-scale by open folds with axis parallel to the SW-dipping stretching lineation. Mancktelow (1992) showed that these folds are contemporaneous to early stages of the SFZ activity.

The hanging wall preserves older structures, showing metamorphic deformations corresponding to four different regional folding phases predating the SFZ (e.g. Keller et al., 2005; Maxelon and Mancktelow, 2005; Steck, 2008). These must not be confused with folds in the footwall, which are contemporaneous with the SFZ.

Based on these evidences, two different models have been proposed. Mancel and Merle (1987) and Steck (1987, 2008) favour a longer-lasting evolution with a major regional shearing phase during the Oligocene, responsible of a large part of the evolution of the SFZ, and a Neogene event of folding of the SFZ and development of the Simplon Line as a narrower, discrete normal fault zone. On the other hand, Mancktelow (1992) holds that both the broad mylonitic belt of the SFZ and the lower grade mylonites and cataclasites close to the SL brittle detachment developed seamlessly during a continuous tectonic event, as suggested by all these structures showing the same lineation and kinematics.

Grasemann and Mancktelow (1993) interpreted the transition from ductile to brittle behaviour as the result of the footwall exhumation. In this model, the ductile shear zone is limited to the footwall (SFZ). Radiometric ages summarized by both Grasemann and Mancktelow (1993) and Campani et al. (2010b) show that the differential exhumation of the footwall with respect to the hanging wall, and hence the SFZ activity, lasted from c. 18 to 4-5 Ma. Muscovite grown in veins from the amphibolite-facies Simplon mylonites took place at 14-14.5 Ma (Campani et al., 2010b), which is taken by the authors as the age of ductile to brittle transition. Fission track ages suggest that displacement along the SL continued until 3-5 Ma, but at lower rates. Grasemann and Mancktelow (1993) also calculated, with their thermal modelling approach, by considering a more or less steady exhumation of the hanging wall contrasting with the variable exhumation rate of the footwall, a total vertical separation along the SFZ of about 15 km, corresponding to an along-dip net slip of 36 km (considering an average dip angle of 25°). Campani et al., (2010a) updated this model by considering (1) a low-angle detachment initially

dipping 30°, (2) a total footwall exhumation between 21 and 27 km and total amount of exhumation for the hanging wall of ca. 12 km, and (3) a variable exhumation and slip rates that decrease at c. 14 Ma.

In any case, the very relevant exhumation of the footwall means that the footwall fault rocks were deformed at different crustal levels under a wide range of temperature conditions (Mancktelow, 1992). As in the fault zone model by Sibson (1977) and Scholz (2002), deformation becomes more localized at lower temperatures, hence higher temperature fault rocks are preserved in the periphery of the SFZ (Mancktelow, 1992), allowing to reconstruct its evolution.

The SFZ is well exposed in large and high-quality outcrops and has been extensively studied (Mancktelow, 1985; Mancktelow, 1992; Mancel and Merle, 1987; Steck, 1987; Steck, 2008; Campani et al., 2010b). In this contribution we will focus on the SL, which is less studied, also because the outcrops are more scarce (Mancktelow, 1985). Mancktelow (1985) describes an outcrop with cataclasites of the SL - consisting of a narrow <10 m cataclastic zone - in Zwischbergental (ZW, Figure 1) , now covered by debris. Also Mancktelow (1992) holds that cataclasites of the SL are principally concentrated in the northwest, where higher exposed structural levels are exposed. Zwingmann and Mancktelow (2004) use a fault gouge layer from the main fault plane of the SL, collected in Zwischbergen (ZW, Figure 1) for radiometric dating. In the following we will describe additional outcrops of cataclasites of the SL that we have found in the last years.

Finally, brittle deformations in the larger Simplonpass area, both in the footwall and hanging wall of the SL, have been studied by Grosjean et al. (2004), who concentrated their analysis mainly on minor Andersonian faults that can be used for stress inversion studies. According to these authors and to Massironi et al. (2011), the paleo-stress that was active during the activity of the SL is characterized by $\sigma_1 = 090/85$ (trend/plunge), $\sigma_2 = 325/30$ and $\sigma_3 = 241/04$ and a stress ratio. $\Phi = (\sigma_2 - \sigma_3)/(\sigma_1 - \sigma_3) \approx 0.5$. Under these conditions the SL must be considered a relatively weak fault (Massironi et al., 2011) according to the definition by Rice (1992).
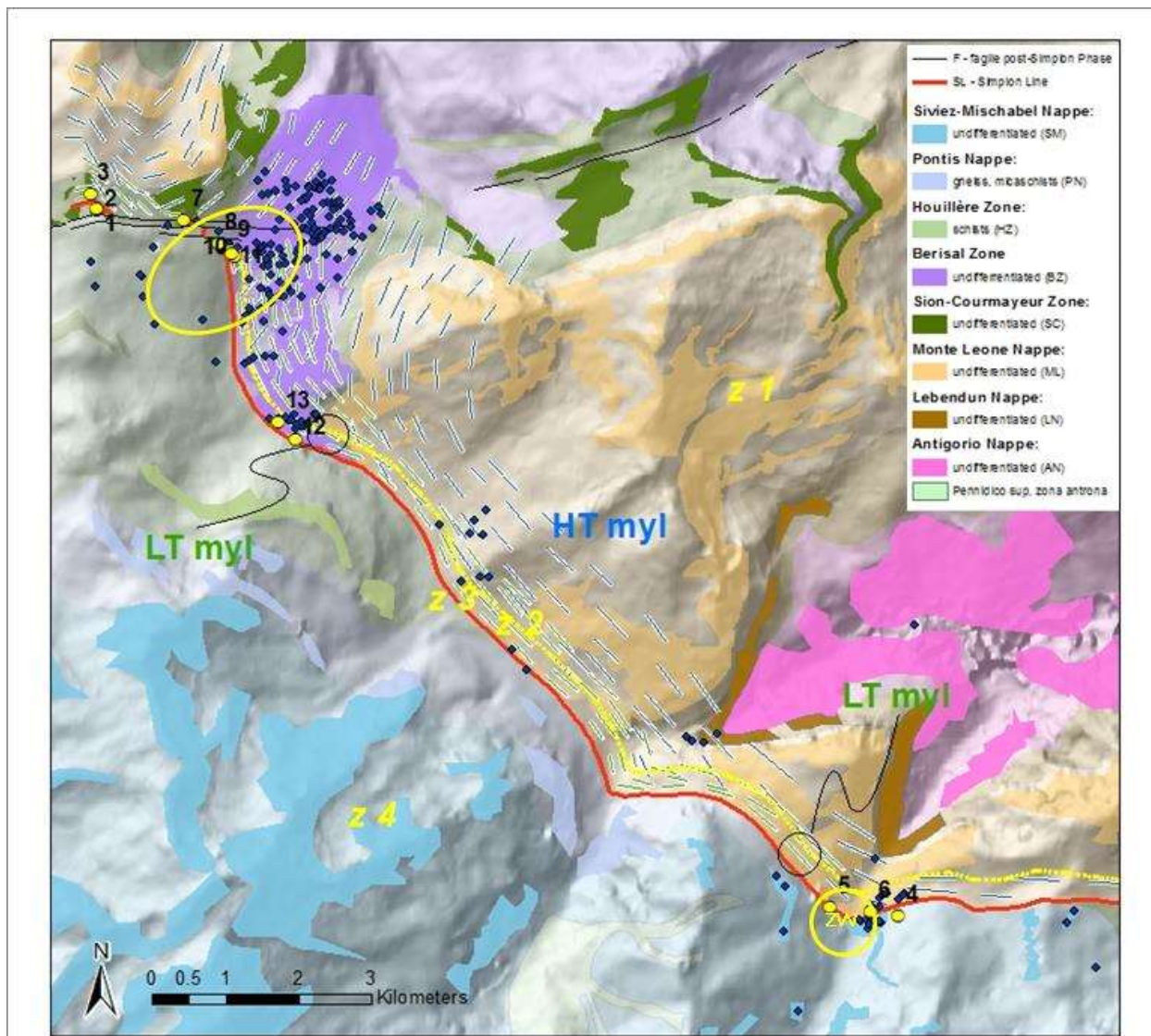
Figure 1 The Simplon Fault Zone (SFZ). (a) Tectonic setting of the Simplon Pass Area (Bistacchi at al, 2012);. The trace of the Simplon Line (in red) crosscut by younger east–west normal faults (in black). The evidences of foliation: low-temperature SFZ mylonitic foliation (LT myl, in green) and the higher-temperature mylonites (HT myl, in blue). Tectonic units as follows. Middle Penninic (Grand San Bernhard System): Siviez-Mischabel (SM), Pontis Nappe (PN),Houillère Zone (HZ), Berisal Zone (BZ). Outer Penninic: Sion-Courmayeur Zone (SC). Lower Penninic (Ossola–Tessin window): Monte Leone Nappe (ML), Lebendun Nappe (LN), Antigorio Nappe (AN). (b) The Simplon Pass area with pointed out the 4 zones described in the text: (z1) high-temperature mylonite, (z2) low- temperature mylonite, (z3) damage zone, (z4) hangingwall; and the two area more studied: Straffelgrat (STG) and Zwischbergental (ZW) .

1.4   Structural analysis

In this study we focus on the final brittle evolution of the SL, which can be reconstructed in some selected outcrops in the Simplon Pass- Staffelgrat and Zwischbergental areas (STG, and ZW in Figure 1). In the following we will subdivide the SFZ in 4 zones, from the more distal footwall rocks (zone1) to the hanging wall (zone4), as in Figure 1 and Figure2.

In all outcrops the contrast between hanging wall and footwall fault rocks and minor structures is evident. The footwall rocks, belonging to the Lepontine Dome, are the mylonites that recorded the deformation history of the SFZ. Distinctive structural elements are the foliation Sm and lineation Lm (Mancktelow, 1985). In the studied outcrops they show an attitude, on average, of 246/23 (dip azimuth/dip) and 244/21 (trend/plunge) respectively (Figure 3a and Figure 3b). Footwall rocks are mainly mylonitic orthogneiss and paragneiss and only marginally calcschists and marbles. In this study the subordinate carbonatic rocks are not considered. In gneiss, phyllosilicates vary between 20-25% and 40-45% (Bistacchi et al., 2012) and are represented by muscovite and biotite for the high temperature mylonites (zone 1), and by muscovite and chlorite for the lower temperature rocks (zone 2 and 3). In the hanging wall (zone 4) we have mainly paragneiss, generally crenulated or folded at the meso-scale, with minor amphibolites and marbles. Some slices of carbonatic rocks can be found along the SL (Bearth, 1972), but they are not investigated in details in this study.

1.5   Up-to-date map of the SL

In Figure 1 we present an updated map of the SL. Our map is in general consistent with the excellent 1:25.000 map by Bearth (1972) and with sketches in Mancktelow (1985), Mancktelow (1990), Mancktelow (1992) and (Campani et al., 2010b), with an exception in the area to the E of the Staffelgrat. This is the area where the SL terminated abruptly in Figure 1 by Bearth (1956), possibly the area indicated as "Rielti Fault" in Mancktelow (1985), and the "area IV" in Campani et al (2010b) where an abrupt change in attitude of the SL is implied. As shown at location 1, 2,3 and in Figure 1, our recent mapping revealed that in this area the trace of the SL is offset with an apparent sinistral separation of c. 1 km by an array of S-dipping more recent normal faults, post-dating the SL. The apparent sinistral separation is a result of normal dip-slip kinematics on S-dipping faults affecting the SW-dipping SL. These S-dipping normal faults can be

attributed to the last deformation phase recognized by Grosjean et al. (2004), and have been detected also a few kilometers to the E, along the Simplon Railway Tunnel, by Pignalosa et al., 2010. The cross-cutting relationships revealed by our updated map shown in Figure 1 are the proof of a deformation event post-dating the SL activity. The key outcrop on which our study is based are indicated in the map of the SL (Figure 1). The SFZ and the SL damage zone outcrop with a remarkeable continuity. However, at the time of writing just one outcrop (to the E of Staffelgrat, STG Figure 1) includes also the fault core (more easily eroded than other rocks). Another outcrop along a mountain road in Zwischbergental, (point 6, Figure 1) was described by Mancktelow (1990) as exposing the fault core, but some debris covered the relevant section, and unfortunately the exposure is no more complete

In the next sections we will describe the different structural domains of the SFZ, starting from the distal hanging wall rocks in zone 1, constituted by the distal high temperature mylonites, and then, approaching the SL, we will continue with zone 2, with low temperature mylonites; then we will jump to zone 4 – the hanging wall rocks, and we will conclude with zone 3 - the fault core.

1.6 High Temperature mylonites of the SFZ (Zone 1)

We present no new findings on this zone, that was extensively studied, amongst others, by Mancktelow (1990), Mancktelow (1992) and Campani et al. (2010b), but we summarize the most important observations in order to provide a complete picture of the fault zone. High temperature mylonites outcrop at distances between c. 1200 and 200 m from the SL (Figure 1 and Figure 2) and show mineral assemblages attributed to the higher-temperature facies (Mancktelow, 1992). These rocks record the earlier and higher-temperature stage of activity of the SFZ. During their exhumation they have been preserved from more recent deformations because the SFZ became more localized up-dip, hence external portions of the shear zone were not affected by shallow deformations (Mancktelow, 1992).

The pervasive mylonitic foliation Sm is defined by the alternation of quartz layers and phyllosilicate films, showing an average attitude of 264/23 (dip azimuth/dip; Figure 3c), with a perfectly along-dip mylonitic lineation Lm marked by quartz ribbons and phyllosilicate aggregates. As described by Mancktelow (1990), quartz ribbons record the relatively high

temperature deformation, showing a bimodal grain size distribution attributed to dynamic recrystallization due to grain boundary migration (GBM) followed by subgrain rotation recrystallization (SGR) at temperatures progressively decreasing, during exhumation, from c. 550°C to c. 450° C. S/C/C' shear bands, porphyroclastic systems and mica fishes (Figure 4a) represent common kinematic indicators in these rocks, confirming the normal, almost perfectly dip-slip kinematics.

Brittle structures recognized in Zone 1, and attributed to the extensional phase responsible for the SL, include high-angle conjugated joints and minor fault planes with average attitude 255/56 and 057/52 (dip azimuth/dip, Figure 5) and normal dip-slip kinematics evidenced by quartz and/or chlorite coatings on slickensides. These minor faults have been used for stress inversion by Grosjean et al. (2004) and Massironi et al. (2011).

1.7 Low temperature mylonites of the SFZ (Zone 2)

Lower-temperature greenschist facies mylonites outcrop in the area between the more distal high-temperature mylonites (zone 1) and the SL (zone 3), hence at distances of up to c. 200 m from the SL, where the brittle deformation is localized. The typical mineral assemblage in both ortogneiss and paragneiss is given by quartz, feldspar, muscovite, and minor chlorite, epidote and titanite; both biotite and garnet porphyroclasts are present. The mylonitic foliation Sm shows an average attitude of 24/224 (dip azimuth/dip, Figure3d) and characterized by a typical lepidoblastic fabric, given by alternating quartz/feldspar lithons and anastomosing phyllosilicate films (muscovite, chlorite, and biotite relics from zone 1 mylonites, Figure 6 and Figure 4b). In the following we will discuss the importance, in terms of mechanical anisotropy in the brittle field, of the arrangement of phyllosilicates in a lepidoblastic fabric, characterized by the shape and lattice and shape preferred orientation of phyllosilicates that are organized in discrete and continuous layers (Figure 4b). S/C, S/C' and S/C/C' shear bands are almost always present and very penetrative (Figure 6), with average attitude 232/32 and 235/43 (dip azimuth/dip) for C and C' planes respectively (Figure 3e and 3f), consistent with dip-slip normal-fault kinematics. Sometimes mica-fishes seem to influence the loci where C' surfaces nucleate .

As already evidenced by Mancktelow (1990), also in zone 2 quartz ribbons and veins are characterized by a bimodal grain size distribution. Dynamic recrystallization developed first by subgrain rotation recrystallization (SGR), but the most pervasive recrystallization event is represented by small grains necleating along grain boundaries by bulging recrystallization (BLG, Stipp et al., 2002). BLG recrystallization, together with the decreasing in SGR, reveal temperature progressively decreasing, during exhumation, from c. 450°C to c. 300° C (Mancktelov, 1990, Stipp 2002).
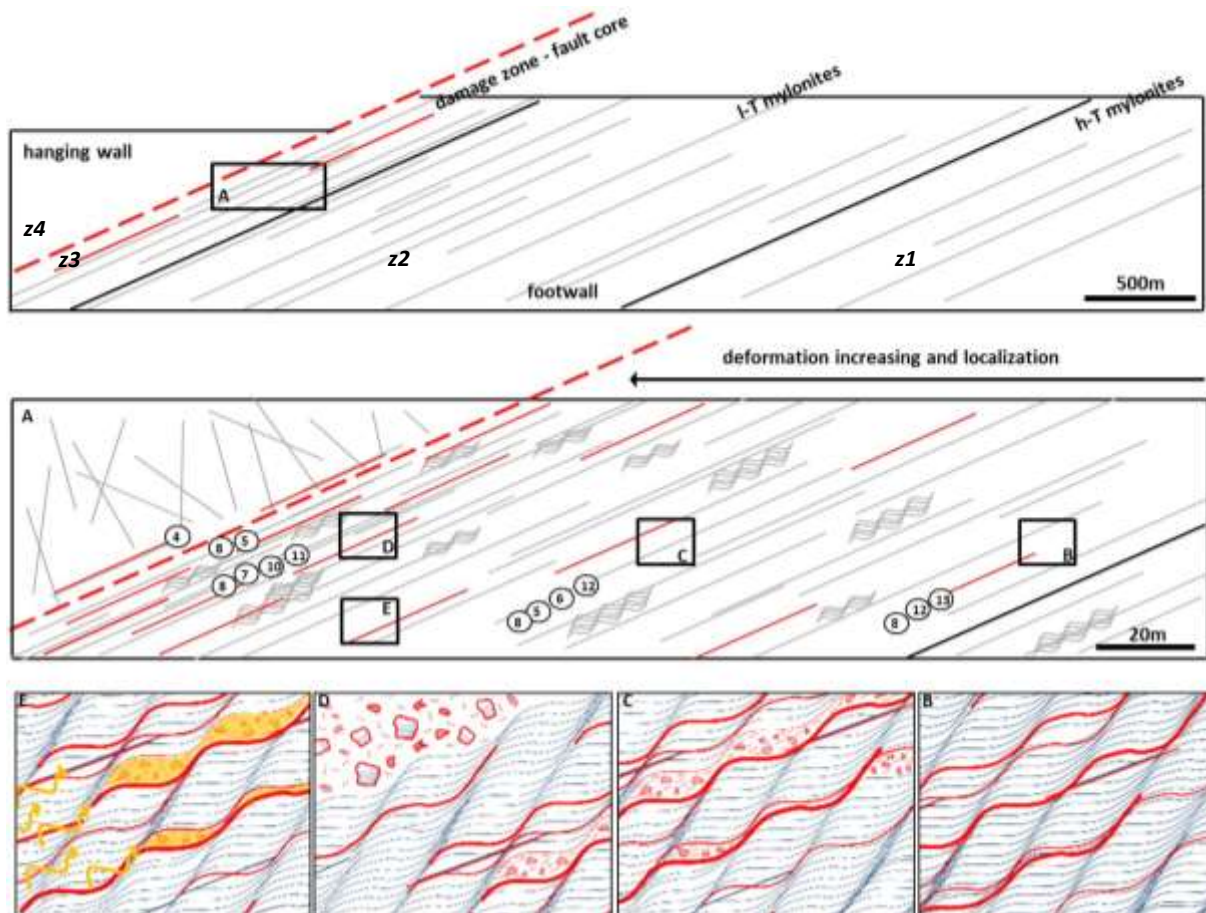
Figure 2 Sketch of the SFZ from SW to NE. (a) Differences between footwall and hangingwall rocks due to differential exhumation. The footwall foliation is consistent with the SL dip. (b) Localization of deformation in the footwall with the presence of high temperature mylonites (HT), characterized by biotit and quartz recrystallization as subgrain rotation recrystallization, low temperature mylonites (LT) with chlorite and bulging quartz recrystallization, and finally the damage zone. (A) Localization of brittle deformation at the SL: the number mark outcrop localization in Figure 1. (B), (C), (D) and (E), show the detail of progressive deformation: (B) protocataclasite with the nucleation of deformation along S/C planes; (C)thickening of cataclastic plane along; (D) overprinting of mylonitic fabric, with the presence of mylonitic clasts in cataclasites, (E) carbonate rich fluids circulation exploiting cataclasite permeability.

1.8   Hanging wall rocks (zone 4)

In contrast with footwall mylonites, hanging wall rocks do not record ductile deformation related to the SFZ in the Simplonpass and Zwischbergental areas (Mancktelow, 1992). These rocks, belonging to Upper Penninic units (Dal Piaz et al., 2003), have undergone pervasive Alpine deformation and metamorphism, but were already exhumed when the activity of the SFZ begun (Grasemann and Mancktelow, 1993). The thickness of hanging wall rocks involved in the SFZ deformation is much less than that in the footwall and corresponds to the damage zone of the brittle SL (Mancktelow, 1990; Campani et al., 2010b).

Here we describe typical hanging wall paragneiss from the Zwischbergental (Figure 1 and Figure2 point 4). The mineral assemblage, developed under greenschist facies conditions, is given by quartz, feldspar, muscovite, chlorite, epidote, and biotite porphyroclasts. Contrastingly with footwall rocks, the hanging wall rocks do not show a mylonitic foliation and/or a penetrative metamorphic fabric associated to the SFZ activity (e.g. quartz veins are not deformed as in the footwall, Mancktelow, 1990), but an older foliation affected (Figure 5a) by penetrative folding. On the other hand, the hanging wall damage zone is characterized by frequent and penetrative brittle structures related to the SFZ: meso-scale faults, joints (Figure 5b), veins, generally showing an intermediate to high dip angle and a rather disperse dip azimuth in the NE and SW quadrants.

Microstructural analysis reveals a markedly different fabric with respect to footwall mylonites: quartz in lithons is characterized by equigranular crystals with a grain size of c. 200 µm, without evidences of the recrystallization processes typical of zones 1 and 2; phyllosilicates are represented by white mica and chlorite flakes with up to 500 µm grainsize (Figure 4h)
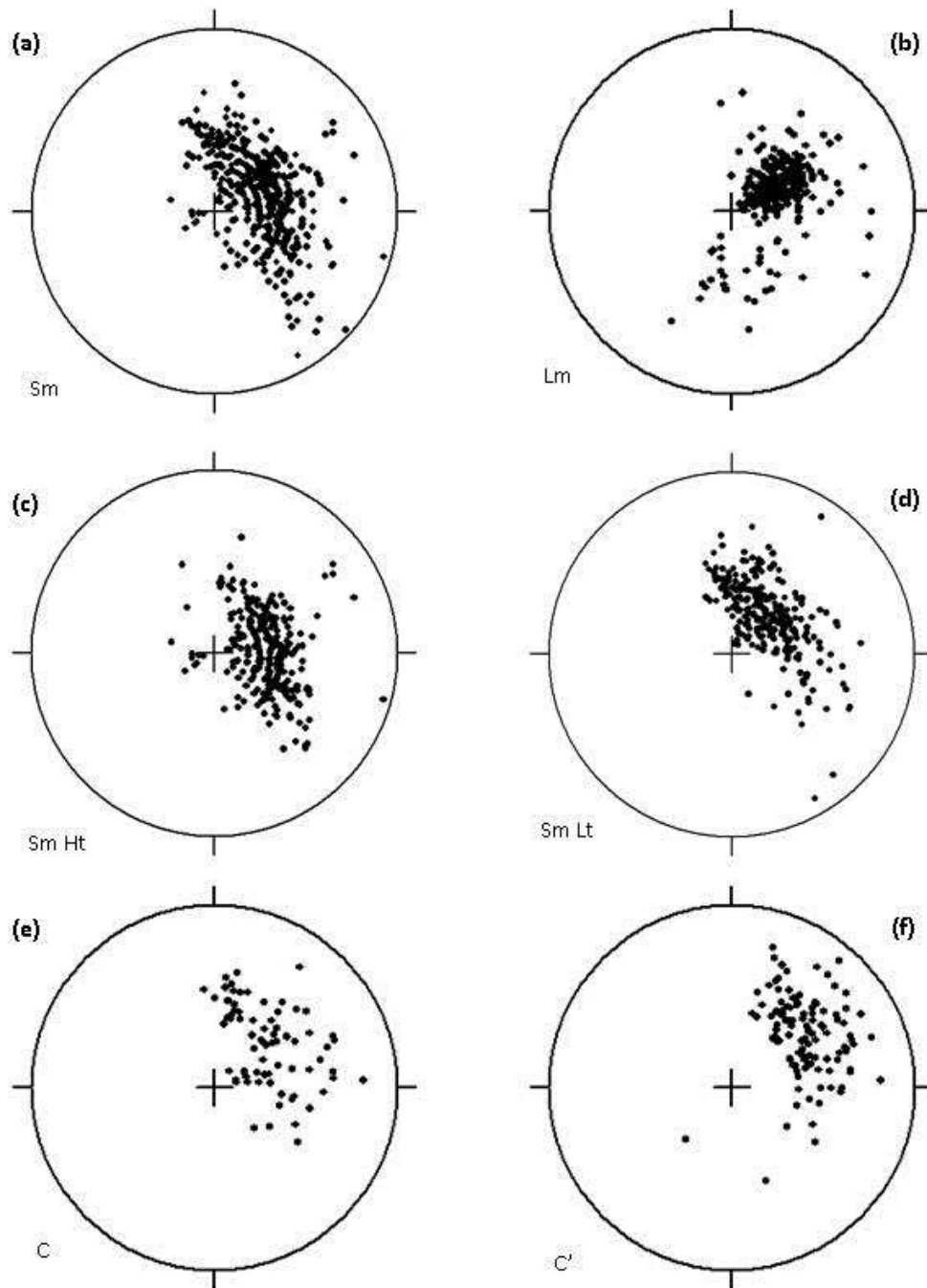
Figure 3 Plots showing the data in the footwall. Plots (a) and (b) show the average dip-dip orientation of (a) foliation Sm (246/23) and (b) lineation Lm (244/21) in the whole footwall area; plot (c) shows foliation in the footwall area characterized by high temperature mylonites (23/264); plots (d), (e) and (f) show the dip dip orientation of (d) foliation Sm (24/224), (e) C planes (32/232) and (f) C' planes (43/235) in low temperature mylonites
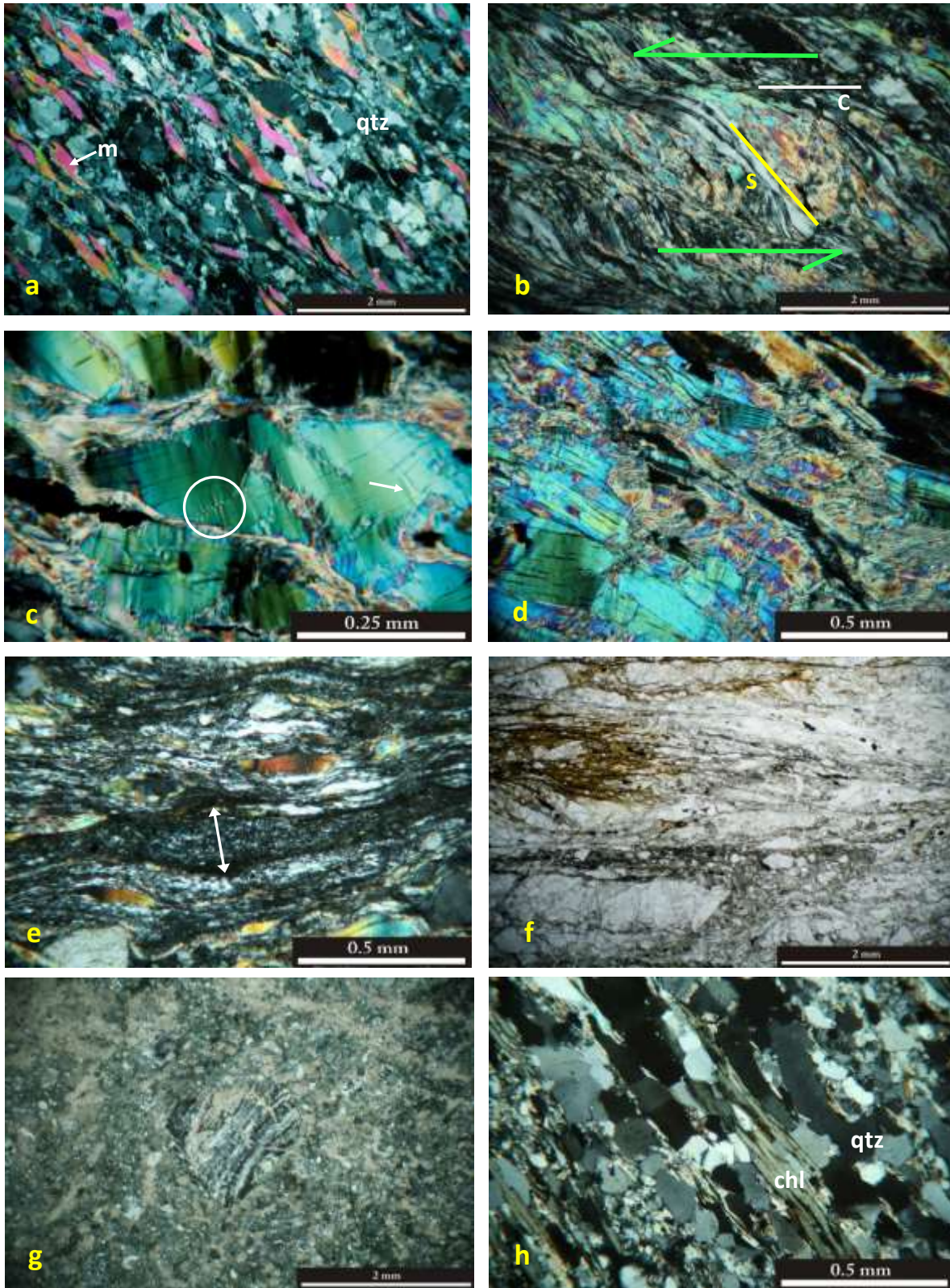
Figure 4 Crossed polarized light images showing the evolution across the SFZ. Pictures from (a) to (g) come from footwall samples and (h) from an hangingwall sample: (a)high temperature mylonites, with a bimodal quartz grain size distribution and micafish-shape porphyroclasts; (b)low temperature mylonites characterized by shear bads ; (c) greenshist mylonites: kink bands inside mica flakes show the first evidences of a brittle deformation ; (d)brittle deformation involving mica layers; (e) thickening of the cataclastic layers along S/C/C' bands; (f) cataclastic sample; (g) cataclastic sample permeated by carbonate rich fluids (h) hangingwall sample, quartz and chlorite

1.9   The brittle SL and its damage zone (zone 3)

This zone is the most proximal to the SL, and includes brittle fault rocks of the damage zone and fault core going from protocataclasites to ultracataclasites, interleaved with less deformed lithons still showing the SFZ mylonites fabric. The structural evolution of the SFZ in the brittle/frictional field has been reconstructed considering oucrops in Zwischbergental (outcrop 5 and, Figure 1 and Figure 2), on the Staffelgrat (outcrop 8, 9, 10, 11), and near Engiloch, along the Diveria (outcrop 12 and 13). In all these outcrops the deformation evolved in a similar way on protoliths represented by greenschist facies mylonitic ortogneiss and paragneiss (zone 2). At Staffelgrat a series composed of calcschists, marbles and chlorite-schists is also present, and in Zwischbergental marbles and dolomitic marbles are present, but these minor carbonatic rock bodies are not considered in this study. In the following we will describe the structural evolution in gneiss, considering a synthetic transect obtained summing up all the observations from the before mentioned outcrops (Figure 2). Thanks to progressive localization of deformation towards the fault core, structures observed farther from the SL are less mature than those in the core, thus we can follow an evolutionary deformation path starting from the outer damage zone, going into the inner damage zone and outer fault core, and eventually reaching the inner fault core (fault rocks classification as in Sibson; 1977, and Scholz; 2002),for a whole thickness of about 80m.

The transition to brittle deformation mechanism, with the development of protocataclasite, correspond to the intensification of mylonitc foliation paragneiss and micaschist and a rock aspect that start to be darker, with brow/grey colors. In the outcrops is possible to recognized centimetric slickenside with striae and sometimes characterized by chlorite fibres growth. At microscale the first protocataclasite appearance is revealed by progressive presence cataclastic seams of 100-300µm (Figure 7a), with a continuity of some millimetres. Fracture nucleation develops exploiting the anastomosing network of shear bands and in particular around the tip of the mica flakes and with the stress increasing, kinking develops in some mica grains and some other crack along [001] mica planes (Figure 4c and d). In contrast with the brittle activation of foliation planes, we notice the total lack of Andersonian conjugated fractures.

Approaching to the SL, rock colour become of a darker grey and the frequency of cataclastic seams increases together with their thickness (Figure 4e and 4f) which reaches also a

centimetric dimension: inside a naked-eye not- recognizable matrix we recognized millimetre angular to subangular quartz clasts. Moreover , some tensional joints (Azimuth/Dip 064°/60°) develop perpendicular to σ3. Microscope observations highlight the presence of angular to sub-angular clasts, with a dimension of about 100µm (Figure 7b), floating in very fine-grained mica matrix, with the dimension of some micrometers which maintain a shape preferred orientation parallel to foliation (Figure 7c). Clasts are composed mainly by fragment of quartz and feldspar rich mylonitic levels, which internally preserve their original fabric.

Loss of all naked-eye rock structures and black colour charatcerized the more deformed rocks (ultracatacalasite). Their angular to sub-angular clasts float in very fine-grained mica matrix, with the dimension of some micrometers and a random orientation (Figure 7d). Cataclastic levels are no more isolated along foliation plans but interconnected, with the development of some fractures or "pull-apart" extension cutting foliation with an high angle. Clasts are both single grains of quartz or feldspar, and polycrystalline clasts of mylonites and their average size is about 50µm, even if some clasts of 500µm are still preserved.

In both cataclasite and ultracataclasite we locally observed the precence of carbonate, proving fluid circulation: they are observed along cataclastic levels, where they seem to circulate by exploting their permeability; or in the pull-apart spaces opened at the interconnection between more cataclastic levels. From these preferred "circulation channels", which form millimetric veins, fluid locally permeate catcalasite and ultracataclasite, overprinting their structures and locally filling millimetre fracture in the more competent clasts.
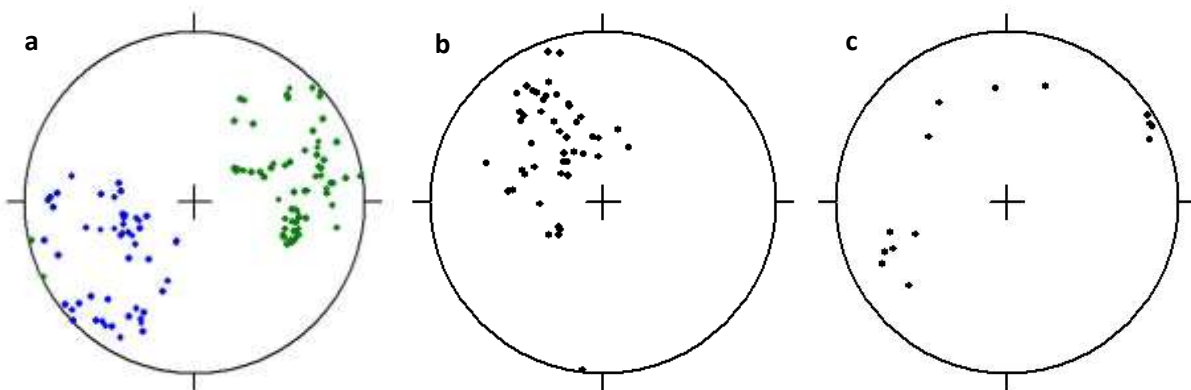

Figure 5 (a) Andersonian conjugate fault set in the footwall high temperature mylonites with a dip dip orientation of 56/255 (green) and 52/057 (blue); (b)hanging wall) foliation planes (42/142); and (2) hanging wall fractures
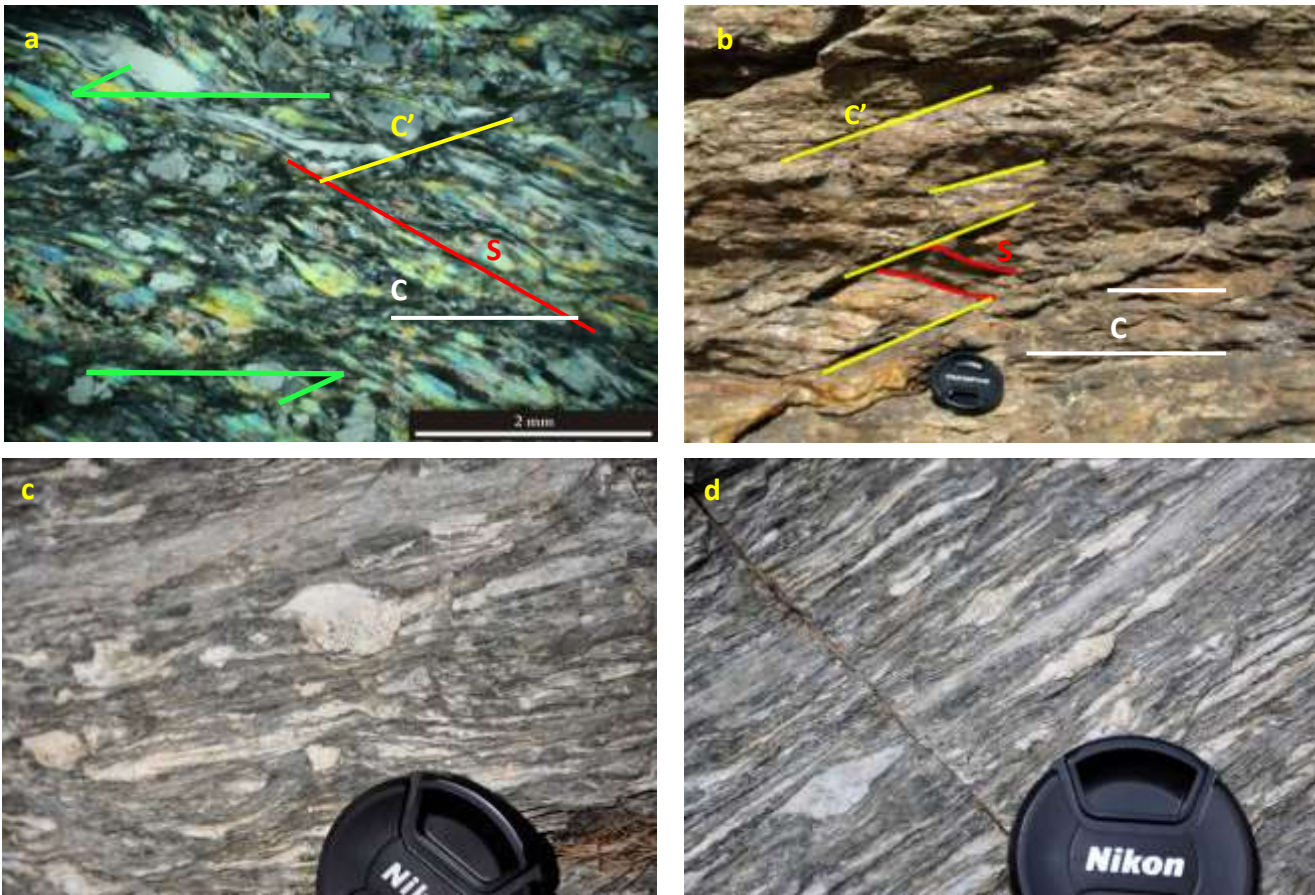
Figure 6(a) Phyllosilicates and quartz layers alternation show the S/C/C' fabric and the shear sense. (b) field evidence of the mylonitic fabric. (c) (d) kinematic indicator and stretched quartz layer. In (c) , to notice the presence of a feldspar σ-porphiroclast

1.10 Discussion

Brittle/frictional deformation along the SFZ is characterized by four main processes: (1) nucleation of microfaults along the phyllosilicate-rich S/C/C' greenschist facies mylonitic foliation, (2) progressive development of a network of cataclastic seams and layers preserving the orientation of the mylonitic foliation; (3) localization of cataclastic deformation in the inner fault core; (4) development of an interconnected flow network in the fault core, allowing fluid access and veining. Noteworthy, (1) no high angle Andersonian structures are present in the fault core and inner damage zone, and (2) veins are frequent in the fault core but their kinematics do not point to hydrofracturing events due to particularly elevated fluid pressure.

The first evidences of nucleation of brittle deformation are concentrated all along the shear bands, and in particular around the tip of the mica flakes, and with the stress increasing kinking develops in some mica grains and some other crack along [001] mica planes. A similar mica behaviour has been observed and described also in labs test performed by Rawling et al. (2002) From these first brittle deformation expressions, rock amount involved in the brittle deformation increases with the implementation of the cataclastic thicknesses along the S/C/C' planes until the deleting of the previous mylonitic fabric, which remains recorded and confined in the greatest mylonitic clasts. We observed a progressive grain size reduction for quartz and feldspar clasts whilst mica fragment matrix, one reach the dimensions of only some micrometers, gradually lost mica grain SPO.

The anisotropy given by foliation allows the development of non-Andersonian planes, whose birth is preferred to the Andersonian one (Figure 2). Figure 8 show stress evolution for anisotropic rocks characterized by weak plane reactivation (Twiss and Moores, 2006), and in particular how their reactivation prevent classical Andersonian fractures to develop. Following the ideal stress path from figure GGb to GGd, built by supposing a constant $\sigma 3$ and an increasing $\sigma 1$, it's possible to recognized foliation reactivation setting: foliation planes, located on Mohr circle by angle Θ, reaches its failure envelop (fig GGd), built by considering an internal friction coefficient of 0.3. Foliation reactivation happens for a stress state that is not critical for the development of Andersonian fracture.

Finally some sample are characterized by the presence of carbonates, showing fluids circulation, which exploited cataclastic layers permeability to circulate and to inject itself in the more competent rock portions. Fluids seem to leak along a anisotropic permeability network (Caine et al., 1996), along cataclasite nucleated along S/C/C' and "critically stressed", and so conductive (Zoback, 2007). Momentary and sudden localized overpressures may induce tensional joint develop and contribute to fault zone weakening with the effective stress drop.
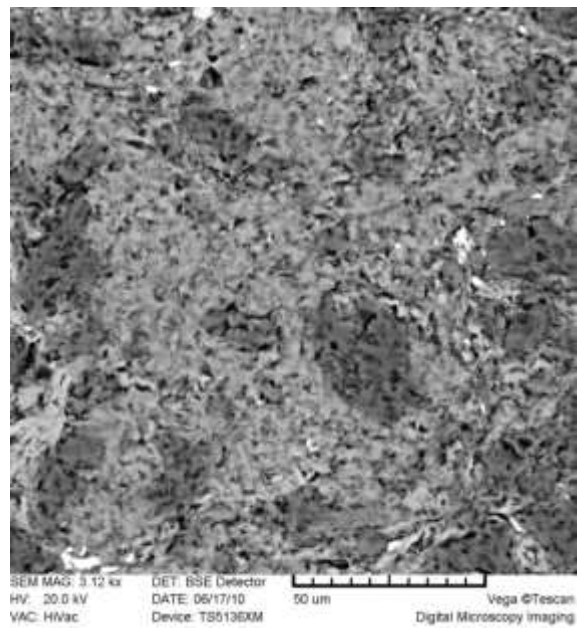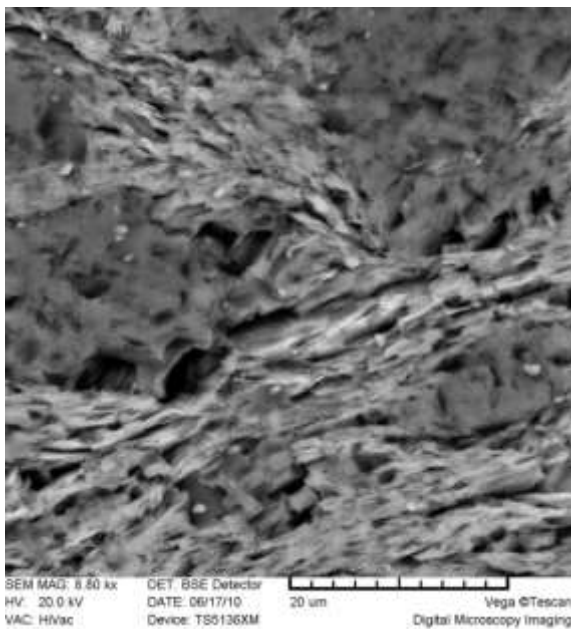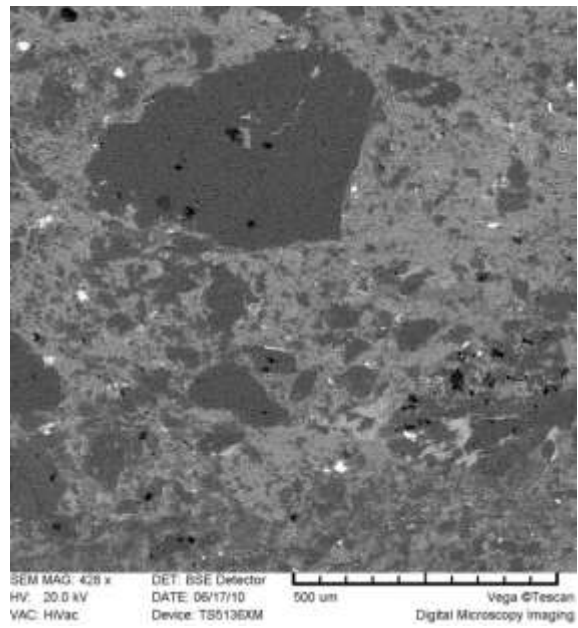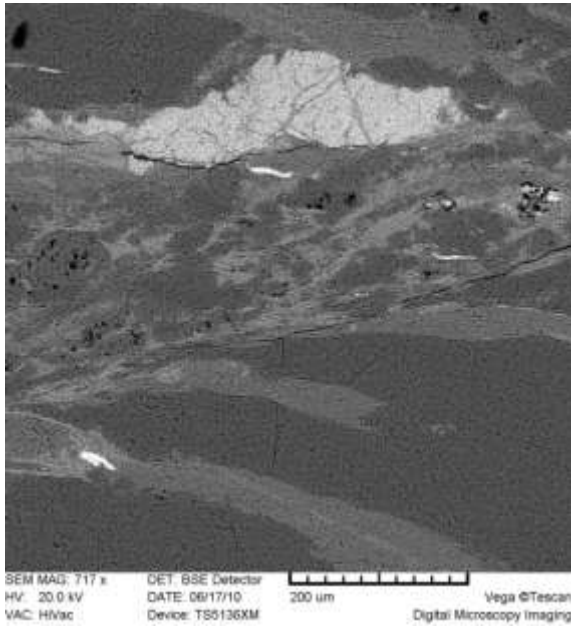
Figure 7 SEM analysis of cataclastic development:(a) cataclastic layer devolp along S/C fabric; (b) thivkemimg of cataclastic layers with a caotic fabric and the typical angular to subangular clasts; (c) phyillosilicates matrix preserve SPO that is finally lost in (d)

1.11 Conclusions

In this contribution we have provided an overview of the brittle deformation of the SL, trying to focus on its nucleation and development, in relationship its anisotropic aspect given by strong phyllosilicate rich foliation. We can resume the main and significant characteristics and this process in few points:

- brittle deformation nucleates along foliation planes where mica is concentrated
- cataclastic layers develop progressively thickening along foliation planes Andersonian fractures don't develop
- carbonate fluids locally impregnate brittle deformed rocks by using cataclastic levels permeability to circulate
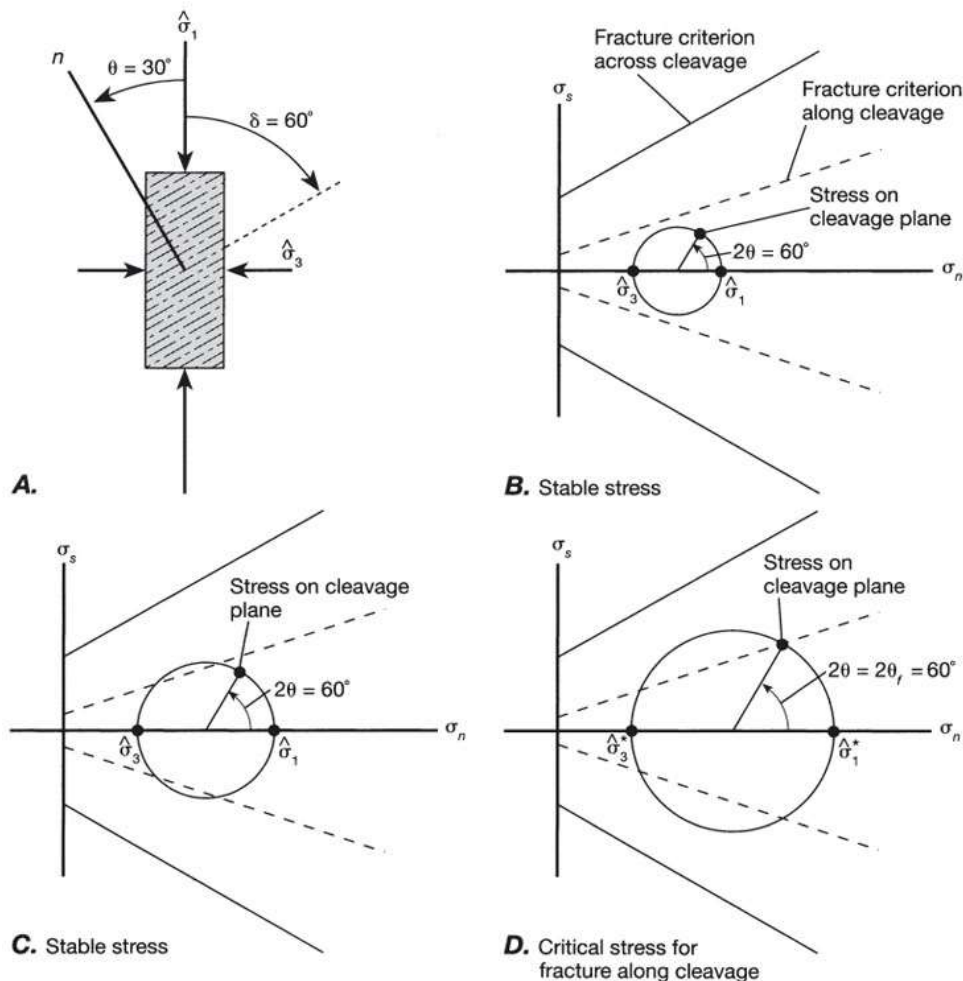
Figure 8 (A) misoriented fault orientation along foliation planes, for an angle with σ1 of about 60° in juxtaposition with Andersonian fracture where θ ~ 30°. From (B) to (D) we can see the "stress path" for the development of weak brittle planes: we can see how the σ1 increasing (C and D), with a constant σ3,allow the cleavage plane to reach its failure envelop (D). we can notice that failure along cleavage happens without the development of Andersonian planes, since the isotropic failure envelop is not reached. (Twiss and Moores, 2006)

These observations illustrate an intrinsic link between rock anisotropy, represented by rock mylonitic fabric foliation, and the development of weak fault planes: anisotropy drives deformation both with the nucleation of brittle deformation along its plane and with the concentration of deformation along its planes, by limiting the development of Andersonian fractures. Fluids circulation appears as secondary and more local weakening mechanism, which develops exploting permeability creating by anisotropic weakening mechanism.

It means that the first important factor determining the development of low angle fault plane is directly link to the presence of pre-existing weak planes, represented by foliation planes riched in phyllosilicates, which act as an important strain attracting factor.

1.12 References

Anderson, E.M., 1905. The dynamics of faulting. Trans. Edinburgh Geol. Soc. 8, 387–402.
doi:10.1144/transed.8.3.387

Bearth, P., 1956. Geologische Beobachtungen im Grenzgebiet der lepontinischen und penninischen
Alpen. Eclogae Geol. Helv. 49, 279–290. doi:10.5169/seals-162078 Nutzungsbedingungen

Bearth, P., 1972. Geologischer Atlas der Schweiz 1:25000 Simplon Atlasblatt 61. Schweizerische
GeologischeKommission.

Bistacchi, A., Massironi, M., Menegon, L., Bolognesi, F., Donghi, V., 2012. On the nucleation of non-
Andersonian faults along phyllosilicate-rich mylonite belts. Geol. Soc. London, Spec. Publ. 367,
185–199. doi:10.1144/SP367.13

Campani, M., Herman, F., Mancktelow, N.S., 2010a. Two- and three-dimensional thermal modeling of a
low-angle detachment: Exhumation history of the Simplon Fault Zone, central Alps. J. Geophys.
Res. 115, B10420. doi:10.1029/2009JB007036

Campani, M., Mancktelow, N.S., Seward, D., Rolland, Y., Müller, W., Guerra, I., 2010b. Geochronological
evidence for continuous exhumation through the ductile-brittle transition along a crustal-scale
low-angle normal fault: Simplon Fault Zone, central Alps. Tectonics 29, TC3002.
doi:10.1029/2009TC002582

Collettini, C., De Paola, N., Holdsworth, R.E., Barchi, M.R., 2006. The development and behaviour of low-
angle normal faults during Cenozoic asymmetric extension in the Northern Apennines, Italy. J.
Struct. Geol. 28, 333–352. doi:10.1016/j.jsg.2005.10.003

Collettini, C., Niemeijer, A., Viti, C., Marone, C., 2009. Fault zone fabric and fault weakness. Nature 462,
907–10. doi:10.1038/nature08585

Collettini, C., Viti, C., Smith, S. a. F., Holdsworth, R.E., 2009. Development of interconnected talc
networks and weakening of continental low-angle normal faults. Geology 37, 567–570.
doi:10.1130/G25645A.1

Dal Piaz, G.V., Bistacchi, A., Massironi, M., Piaz, V.D., Geologia, D., Geofisica, P., Padova, U., 2003.
Geological outline of the Alps. Episodes 26, 175–180.

Dean, S.M., Minshull, T. a., Whitmarsh, R.B., 2008. Seismic constraints on the three-dimensional
geometry of low-angle intracrustal reflectors in the Southern Iberia Abyssal Plain. Geophys. J. Int.
175, 571–586. doi:10.1111/j.1365-246X.2008.03869.x

Grasemann, B., Mancktelow, N.S., 1993. Two-dimensional thermal modelling of normal faulting: the
Simplon Fault Zone, Central Alps, Switzerland. Tectonophysics 225, 155–165. doi:10.1016/0040-
1951(93)90277-Q

Grosjean, G., Sue, C., Burkhard, M., 2004. Late Neogene extension in the vicinity of the Simplon fault zone (central Alps, Switzerland). Eclogae Geol. Helv. 97, 33–46. doi:10.1007/s00015-004-1114-9

Handy, M.R., 1990. The solid-state flow of polymineralic rocks. J. Geophys. Res. 95, 8647–8661.

Holdsworth, R.E., van Diggelen, E.W.E., Spiers, C.J., de Bresser, J.H.P., Walker, R.J., Bowen, L., 2011. Fault rocks from the SAFOD core samples: Implications for weakening at shallow depths along the San Andreas Fault, California. J. Struct. Geol. 33, 132–144. doi:10.1016/j.jsg.2010.11.010

Jaeger, J.C., Cook, N.G.W., Zimmerman, R.W., 2007. Fundamentals of Rock Mechanics, 4th editio. ed. Wiley-Blackwell.

Keller, L.M., Hess, M., Fügenschuh, B., Schmid, S.M., 2005. Structural and metamorphic evolution of the Camughera – Moncucco, Antrona and Monte Rosa units southwest of the Simplon line,Western Alps, Eclogae Geologicae Helvetiae. doi:10.1007/s00015-005-1149-6

Kronenberg, A.K., Kirby, S.H., Pinkston, J., 1990. Basal slip and mechanical anisotropy of biotite. J. Geophys. Res. 95, 19257. doi:10.1029/JB095iB12p19257

Lecomte, E., Jolivet, L., Lacombe, O., Denèle, Y., Labrousse, L., Le Pourhiet, L., 2010. Geometry and kinematics of Mykonos detachment, Cyclades, Greece: Evidence for slip at shallow dip. Tectonics 29, n/a–n/a. doi:10.1029/2009TC002564

Lecomte, E., Le Pourhiet, L., Lacombe, O., Jolivet, L., 2011. A continuum mechanics approach to quantify brittle strain on weak faults: application to the extensional reactivation of shallow dipping discontinuities. Geophys. J. Int. 184, 1–11. doi:10.1111/j.1365-246X.2010.04821.x

Mancel, P., Merle, O., 1987. Kinematics of the northern part of the Simplon line (Central Alps). Tectonophysics 135, 265–275. doi:10.1016/0040-1951(87)90111-9

Mancktelow, N.S., 1985. The Simplon Line: a major displacement zone in the western Lepontine Alps. Eclogae Geol. Helv. 78, 73–96.

Mancktelow, N.S., 1990. The Simplon Fault Zone.

Mancktelow, N.S., 1992. Neogene lateral extension during convergence in the Central Alps: Evidence from interrelated faulting and backfolding around the Simplonpass (Switzerland). Tectonophysics 215, 295–317. doi:10.1016/0040-1951(92)90358-D

Massironi, M., Bistacchi, A., Menegon, L., 2011. Misoriented faults in exhumed metamorphic complexes: Rule or exception? Earth Planet. Sci. Lett. 307, 233–239. doi:10.1016/j.epsl.2011.04.041

Maxelon, M., Mancktelow, N.S., 2005. Three-dimensional geometry and tectonostratigraphy of the Pennine zone, Central Alps, Switzerland and Northern Italy. Earth-Science Rev. 71, 171–227. doi:10.1016/j.earscirev.2005.01.003

Moore, D.E., Rymer, M.J., 2007. Talc-bearing serpentinite and the creeping section of the San Andreas fault. Nature 448, 795–7. doi:10.1038/nature06064

Pignalosa, A., Zattin, M., Massironi, M., Cavazza, W., 2010. Thermochronological evidence for a late Pliocene climate-induced erosion rate increase in the Alps. Int. J. Earth Sci. 100, 847–859. doi:10.1007/s00531-010-0510-9

Rawling, G.C., 2002. Dilatancy, brittle strength, and anisotropy of foliated rocks: Experimental deformation and micromechanical modeling. J. Geophys. Res. 107, 2234. doi:10.1029/2001JB000472

Rice, J.R., 1992. Fault stress states, pore pressure distributions, and the weakness of the San Andreas Fault, in: Wong, T. (Ed.), Fault Mechanics and Transport Properties of Rocks. Academic Press, pp. 475–503.

Scholz, C.H., 2002. The mechanics of earthquakes and faulting. Cambridge University Press.

Shea, W.T., Kronenberg, A.K., 1993. Strength and anisotropy of foliated rocks with varied mica contents 15.

Sibson, R.H., 1977. Fault rocks and fault mechanisms. J. Geol. Soc. London. 133, 191–213. doi:10.1144/gsjgs.133.3.0191

Sibson, R.H., 1985. A note on fault reactivation. J. Struct. Geol. 7, 751–754. doi:10.1016/0191-8141(85)90150-6

Steck, A., 1987. Le massif du Simplon - Réflexions sur la cinématique des nappes de gneiss. Schweizerische Mineral. Petrogr. Mitteilungen 67, 27–45. doi:10.5169/seals-51585

Steck, A., 2008. Tectonics of the Simplon massif and Lepontine gneiss dome: deformation structures due to collision between the underthrusting European plate and the Adriatic indenter. Swiss J. Geosci. 101, 515–546. doi:10.1007/s00015-008-1283-z

Steck, A., Hunziker, J.C., 1994. The Tertiary structural and thermal evolution of the central Alps compressional and extensional structures in an orogenic belt. Tectonophysics 238, 229–254.

Van Diggelen, E.W.E., De Bresser, J.H.P., Peach, C.J., Spiers, C.J., 2010. High shear strain behaviour of synthetic muscovite fault gouges under hydrothermal conditions. J. Struct. Geol. 32, 1685–1700. doi:10.1016/j.jsg.2009.08.020

Wernicke, B., 1981. Low-angle normal faults in the Basin and Range Province: nappe tectonics in an extending orogen. Nature 291, 645–648. doi:10.1038/291645a0

Zwingmann, H., Mancktelow, N.S., 2004. Timing of Alpine fault gouges. Earth Planet. Sci. Lett. 223, 415–425. doi:10.1016/j.epsl.2004.04.041

2 The lock-up angle for brittle activation of a phyllosilicate-rich mylonitic fabric (Grandes Rousses Massif, France): implications for friction coefficients

Francesca Bolognesi and Andrea Bistacchi

Department of Earth and Environmental Sciences, Università degli Studi di Milano Bicocca, Italy

2.1 Abstract

One of the possible mechanisms explaining the nucleation and propagation of weak faults showing a non-Andersonian attitude is the mechanical anisotropy of phyllosilicate-rich mylonitic rocks. This allows for faults to slip under an unfavourable normal to shear stress ratio, in contrast to E. M. Anderson's theory of faulting. Here we analyse the mutual orientation of foliation and stress field axes in the specific case of the mylonitic micaschist of Grandes Rousse Massif (France) and discuss the implications in terms of mechanical anisotropy. The brittle reactivation of the mylonitic fabric is limited to some areas, whilst in other areas we observe the development of Andersonian conjugate shear fractures. This different behavior is related to the attitude, and particularly to the dip angle, of the mylonitic fabric. We apply stress inversion and anisotropic slip tendency analysis and propose a lock-up angle for reactivation of the Grandes Rousses schists mylonitic foliation. This angle marks the boundary between a field where the reactivation of preexisting anisotropies is still possible and a field where reactivation is not possible and Andersonian fractures develop. These field observations can be seen as a very large-scale triaxial experiment, which allows to define the ratio of the internal friction coefficient for reactivation of the mylonitic foliation to the isotropic friction coefficient, hence the degree of mechanical anisotropy.

2.2 Introduction

The presence of weak faults, characterized by an unfavorable orientation with respect to the regional stress field according to the Anderson theory of faulting, is quite common in nature, even if it represents an anomaly. Typical misoriented faults are low-angle normal faults (LANFs; Wernicke, 1981), high-angle reverse faults (Cox 1995; Butler et al. 2008) and strike-slip faults forming a high angle to the main compressional stress axis (e.g. the San Andreas Fault; Townend & Zoback 2004).

Different weakening mechanisms have been proposed to explain the brittle activation along misoriented planes: (1) mechanisms involving layers characterized by a the presence of weak minerals, as e.g. phyllosilicates, clays, etc. (Byerlee, 1978), (2) weakening due to high fluid pressure resulting in low effective stress (Hubbert & Rubey, 1959, Sibson 1981, Rice 1992, Faulkner and Rutter, 2001), (3) mechanisms involving a local rotation of principal stress axes in a weak fault zone (Rice, 1992, Faulkner et al., 2006), or finally (4) mechanisms linked to rock mechanical anisotropy (Duveau et al., 1998, Shea and Kronenberg, 1993; Bistacchi et al., 2012).

The effect of anisotropy on deformation is qualitatively well known by all second-year geology students, and reactivation, or just activation, of weakness surfaces like metamorphic foliations, bedding, and fracture sets is very often invoked as a fundamental factor influencing deformation modes or "styles" at all scales (Twiss and Moores, 2006).

However, quantitative studies on the mechanical anisotropy of foliated rocks are confined to laboratory experiments (Attewell & Sandford, 1974; Bell & Coulthard, 1997; Donath, 1961 and 1972; Duveau et al. 1998; McCabe & Koerner, 1975; Walsh & Brace, 1964; Collettini et al., 2009). These experiments highlight how a favorable orientation of anisotropy surfaces induces their brittle activation, and how this results in an internal friction coefficient that is much lower with respect to deformation by nucleation and propagation of newly formed fractures.

Particularly, for a foliation marked by isoriented phyllosilicates, the internal friction coefficient (tangential to normal stress ratio at ropture) shows a marked anisotropy, decreasing from c. 0.7, for new fractures cutting across foliation, to c. 0.3 for fractures exploiting foliation surfaces. If phyllosilicates are organized in continuous films, as in a mylonite with lepidoblastic texture, this behavior is relevant for relatively low phyllosilicate contents (> *c.* 20%). This behavior has been found in experiments on slates (Attewell & Sandford, 1974; Donath, 1961; Walsh & Brace,

1964), laminated clays (Bell & Coulthard, 1997), phyllites (Donath, 1972), chlorite and muscovite schists (Duveau et al. 1998) and phyllonites (Collettini et al., 2009).

In this contribution we develop a new approach, combining paleostress analysis (allowing to define the in-situ stress field at the time of deformation), and a meso- and micro-scale characterization of modes of brittle failure in micaschists of the Grandes Rousses Massif (Helvetic-Dauphinois Domain of the French Alps), which allows us to set up a sort of field-scale triaxial experiment and quantitatively evaluatie the mechanical anisotropy of these rocks at the 10 m to 1 km scale.

2.3   Geological setting

The Grandes Rousses Massif, located in the French Alps (Figure 9), belongs to the Helvetic-Dauphinois domain (Dal Piaz et al., 2003)), composed of thick skinned basement thrust sheets (the "external crystalline massifs") and Mesozoic sedimentary cover units that can be found in deep synclines interleaved between the basement units, or in décollement nappes (Gidon, 1979 and 1999; Ford, 1996, Dumont et al., 2008).

Deformation in the basement units started at least during the Hercynian orogeny. Later on, Paleozoic foliations and shear zones were reactivated during the Jurassic rifting (as normal faults bounding asymmetric sedimentary basins, Barfety & Gidon, 1983; Lemoine et al., 1986), and again from the Late Oligocene, when the Alpine orogeny propagated into what was the European proximal passive margin. Thus the Alpine deformations developed in a heterogeneous material, already deformed during the Paleozoic and Mesozoic, and was influenced by its weakness and anisotropy.

The Grandes Rousses Massif is located between the Belledonne Massif, to the NW, and the Pelvoux Massif, to the SE. The Grandes Rousses and Belledonne represent two fragments of the same basement unit, deformed and isoclinally folded (Boriani et al., 1974).

According to Dumont et al. (2008), during the Alpine deformation the whole Dauphiné domain was involved in a multistage shortening involving both Hercynian basement rocks and Mesozoic sedimentary covers. Particularly, the Grandes Rousses massif records four Alpine folding and thrusting events (Dumont et al., 2008).

We carried out our "field experiment" in the NW part of the Grandes Rousses, to the north of the Pic de l'Étandard, in the glacial hanging valley of the three Saint Sorlin's lakes (Lac Bramant,Lac Blanc and Lac Tournant, Figure 10); this corresponds to the northern extremity of the Grandes Rousses massif (Dumont et al., 2008). The hanging valley was carved by the Saint-Sorlin glacier and it is delimited by two faults: the Saint-Sorlin lake western fault and the Grandes Rousses thrust.

Basement rocks outcropping in the western side of the valley are chlorite and biotite schists with minor garnet amphibolites; rocks outcropping in the eastern side are migmatitic gneiss, showing a mylonitic fabric approaching the contact to the schists Figure 10). Schists and gneiss are separated by a discontinuous slice of strongly deformed meta-sedimentary rocks (Barbier at al, 1977).

Crystalline basement rocks are characterized by a penetrative sub-planar foliation, with average Dip/Dip Direction between 60°/102° and 90°/102°.

Alpine deformation does not result in penetrative metamorphic foliations in this area, but in concentrated deformation along ductile shear zones, as in the mylonites separating the migmatitic gneiss and schists. On the other hand, brittle deformation is penetrative in all the outcrops, and increases in mylonites.

In the following we will discuss the distribution and modes of brittle deformation as a function of pre-existing inherited structures.

Figure 9 Geographycal setting of Grandes Rousses Massif
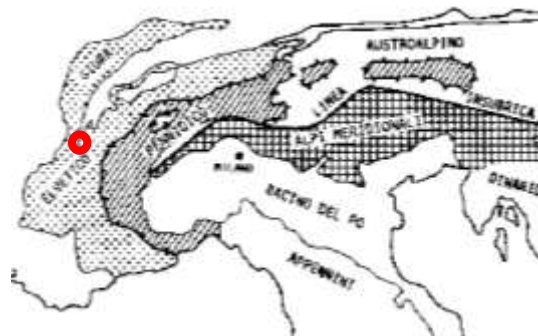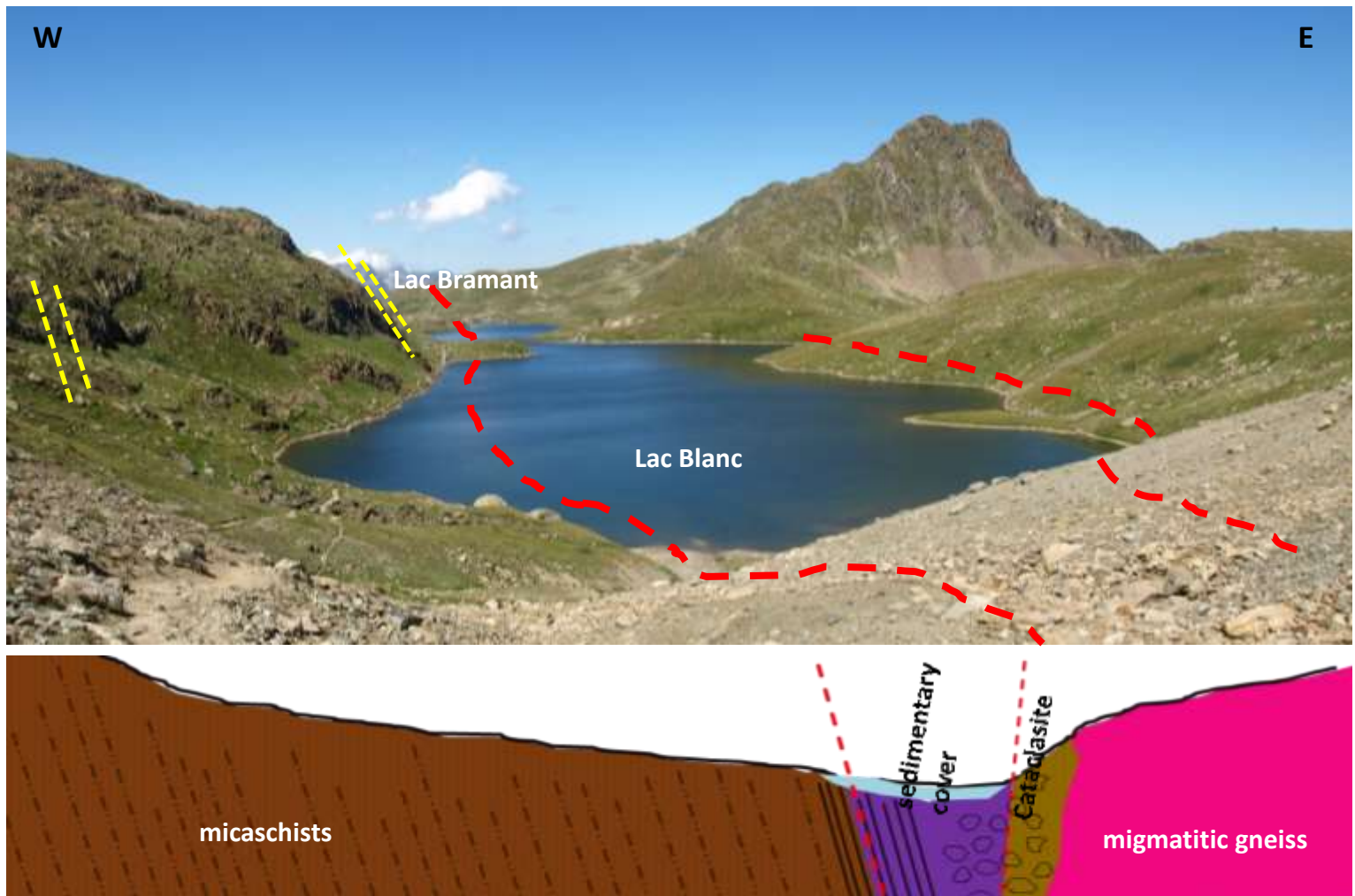
Figure 10 The area of study, developed along Lac Bramant and Lac Blanc. In evidence the presence of the sedimentary cover pinched between basement gneiss and micaschists. A cataclastic level divide the sedimentary cover from the crystalline basement in the E side. Our attention focused on the W side, with better outcrops.

2.4 Mesostructural analysis

Micashists outcropping on the West side of the Saint Sorlin lakes are characterized by a penetrative metamorphic foliation, locally developing in a mylonitic foliation with S/C/C' fabric. This foliation is constituted by an alternation of phyllosilicate films and quartz and feldspar levels, and shows a rather constant dip-direction of ca. 102° (ESE); the dip angle is more variable, going from 60° to 90°, with two maxima at about 65° and 75° (plots in Figure 11,   Figure 12a and Figure 12d).

Alpine deformation develops onto this Hercynian fabric, and is characterized by different brittle structures: cataclastic levels developed along foliation surfaces, conjugated fractures, and tensional joints or quartz-chlorite-sulphide veins.

Tensional joints and veins are present in the whole area; they are represented by arrays of subvertical to vertical fractures (90°/014°, Figure 12a) generally filled with quartz and chlorite fibers (09/013, Figure 12f), and sometimes by sulphide masses. Their trace length varies between some centimeters and some meters, and aperture or vein thickness goes from some millimeters to some centimeters. Conjugated fractures and cataclastic levels developed along the metamorphic foliation are more frequent in areas where the mylonitic fabric is more developed, so roughly along the boundary between migmatitic gneiss and schists.

The presence of these two different "modes of deformation" is generally exclusive, i.e. we observed outcrops characterized by either the exclusive presence of cataclastic levels along foliation, or by the exclusive presence of conjugated fracture, but transitional outcrops characterized by the presence of both deformation modes are very uncommon.

In the following we better characterize the two modes of deformation and their relationship with the foliation dip angle.

Conjugated fractures

We observed conjugated fractures in outcrops characterized by an average dip angle higher than c. 70°, with an average value of c. 75 (75°/102° Figure 11a, b, c, d). They appear as fractures cutting foliation at a high angle and show average attitudes of Dip/Dip Direction 88°/229° and 87°/166° (Figure 11a, b, c, d and Figure 12e). Even if they macroscopically cut the metamorphic foliation, a closer observation highlights more complex mechanisms, since each single fracture is constituted by a stair-stepping sequence of millimetric segments which really crosscut foliation and other millimetric segments exploiting the foliation (Figure 4c). These conjugated fractures are characterized by very small slip, generally in the order of a few millimeters, hence they rarely host kinematic indicators.
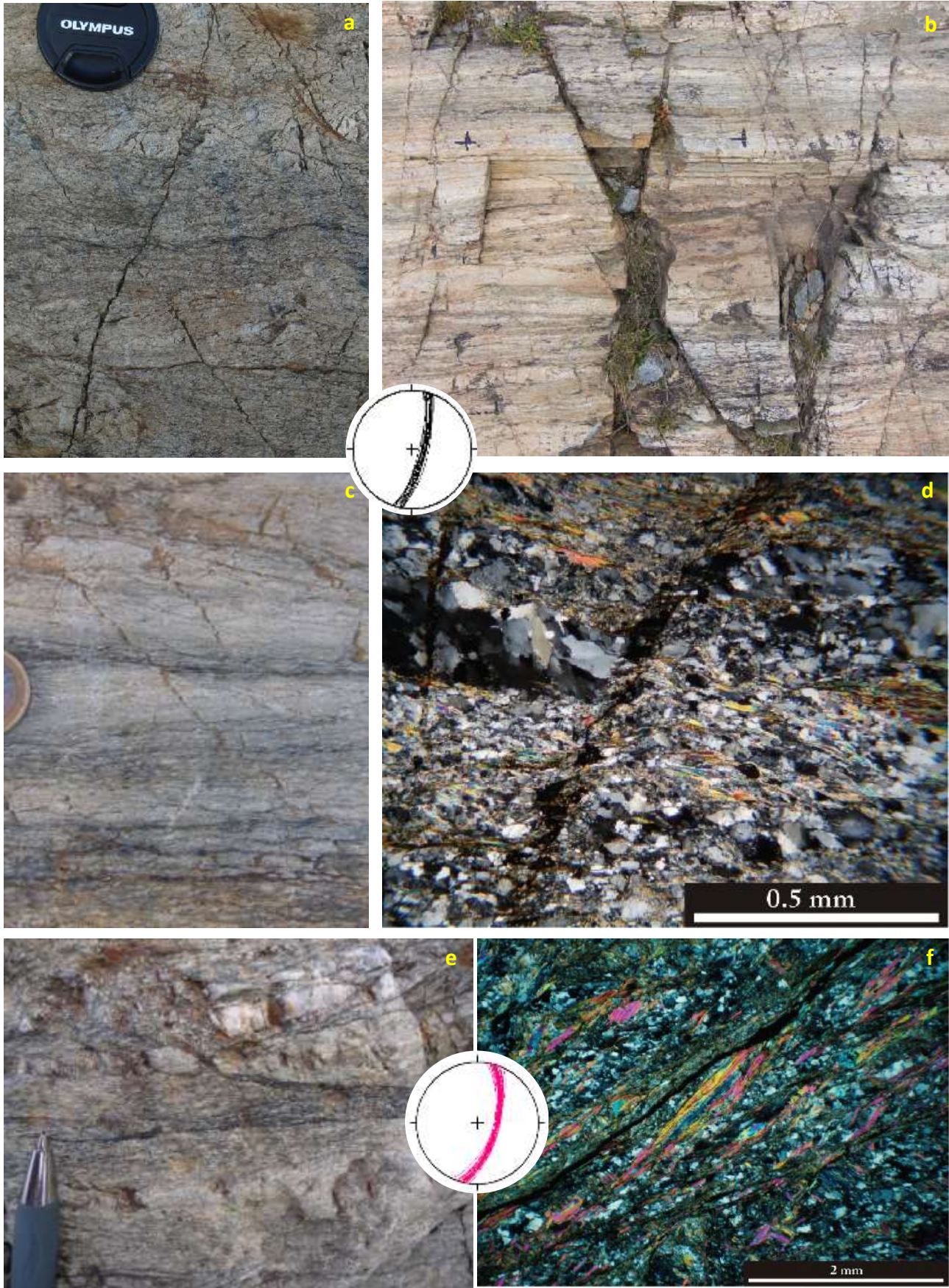
Figure 11 (a) and (b) : conjugated fractures crosscutting foliation; (c) fracture cutting foliation with an high angle composed of segments cutting foliation and short segments running along it; (d) thin section with a fracture cutting foliation; (e) cataclastic levels along foliation planes; (f) fracture along foliation. In the middle of (a), (b), (c) and (d), foliation orientation (75°/102°) where we found them, whilst between (e) and (f) we show foliation orientation (65°/102°) where we observed brittle activation of it
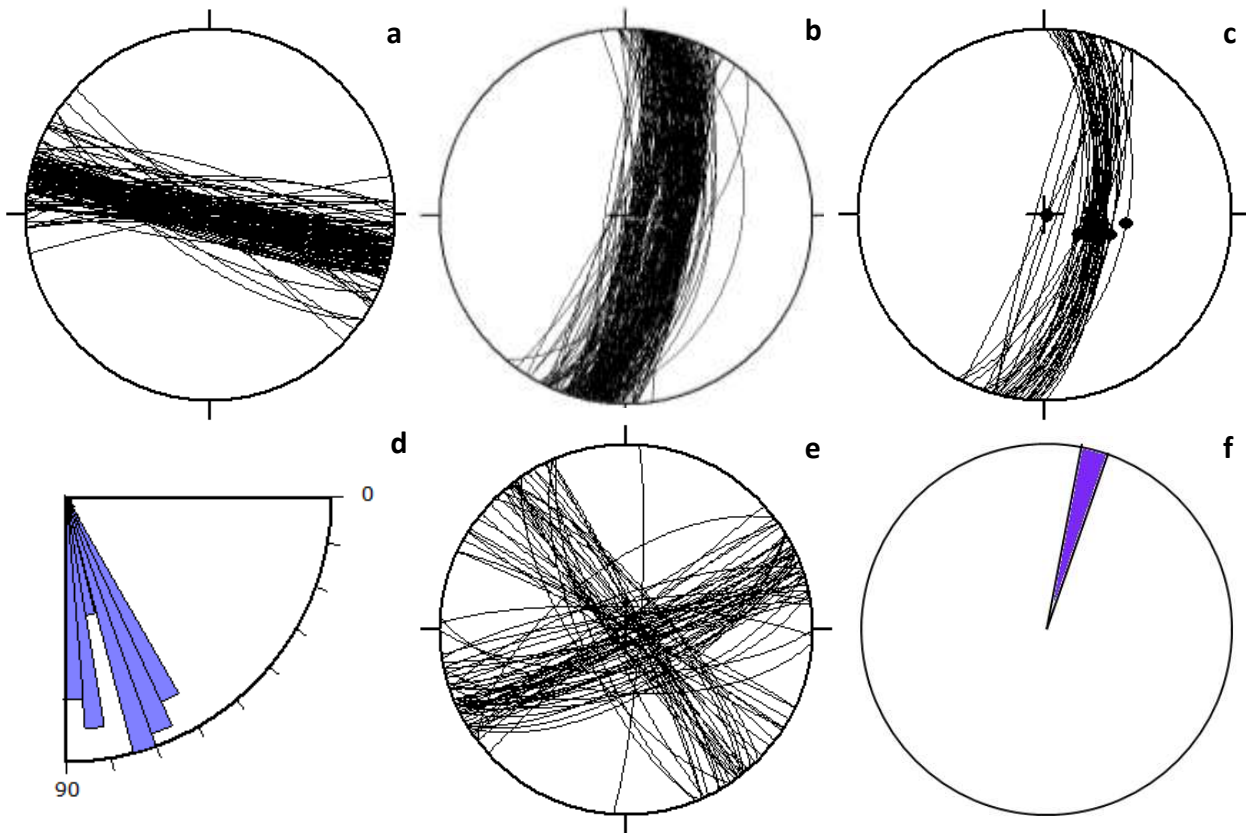
Figure 12 . (a) tensional joints; (b) foliation; (c) brittle deformation along foliation planes; (d) foliation dip angles; (e) Andersonian conjugated fault planes; (f) quartz and chlorite fibers

Cataclastic levels

We observe the development of cataclastic levels exploiting the metamorphic foliation for dip angles lower than c. 70°, with an average value of c. 65° (65°/102° Figure 11e, f and Figure 12c). They develop in outcrops characterized by a penetrative mylonitic fabric or by higher-than-average phyllosilicate content and exploit the weakness of phyllosilicates films that mark the foliation. The cataclasite layers observed on outcrops are generally very thin, in the order of a few millimeters (possibly the detection limit with naked eye), and only in a few cases they are more developed, reaching up to 2 cm of thickness. Slickenside surfaces associated to the cataclasite layers show kinematic indicators (mainly striae and quartz or chlorite fibers), which suggest a sinistral/reverse slip. In a few outcrops we can see the coexistence of cataclasite layers exploiting the foliation and conjugated fractures, but this is not common and generally the transition from one mode of deformation to the other is very abrupt.

2.5 Microstructural analysis

Samples collected for microstructural analysis have been chosen in order to represent the two different modes of deformation and the transition between them. All samples evidence a lepidoblastic foliation given by an alternation of phyllosilicates films/layers and quartz and feldspar levels (Figure 13a), with a shape-preferred orientation of all minerals. Phyllosilicates are represented by muscovite, biotite and chlorite, which partially replaces biotite; we observe both thin films and thicker layers up to some millimeters. Also micafish porphyroclasts are present. Phyllosilicates locally show a progressive orientation rotation forming micro-fold, as proof of previous deformation.

Quartz grains show a bimodal grain size distribution: smaller grains show irregular grain boundaries typical of bulging recrystallization (Figure 13d) and larger grains show diagnostic features of subgrain rotation recrystallizations (Stipp et al., 2002). Along foliation and particularly along local shear bands, quartz grains can be indented or truncated at dark seams of insoluble material, pointing to pressure solution deformation mechanisms.

As at the meso-scale we observed the presence of three different kinds of brittle structuress: tensional joints, shear fractures, and brittle activation of foliation evidenced by thin (ultra)cataclasite layers. Tensional joints/veins develop perpendicular to foliation and are often filled with quartz and chlorite, oxides and less frequently carbonates (Figure 13c). Quartz is arranged in long fibers perpendicular to joint walls (Figure 12f) and it often hosts fluid inclusion trails parallel to fracture boundaries, suggesting a crack and seal opening mechanism (Ramsay, 1980) and a syntaxial vein growth (Durney & Ramsay 1973).

Samples showing in the field the brittle activation of foliation, show the same behavior at the micro-scale, with micro-cracks parallel to foliation (Figure 11e and f) and concentrated in phyllosilicates films, Sometimes, together with simple fractures, we observe thin cataclastic anastomosing micro-faults with ultracataclasite seams some hundreds of micrometers thick. All these structures exploit [001] cleavage in micas or develop at the boundary between phyllosilicates and quartz/feldspar levels.

Similarly, samples dominated in the field by conjugated fractures show a similar behavior at the micro-scale, with fractures cutting foliation at high angle, but locally following a stair-stepping path with high-angle segments cutting the more competent quartz/feldspar levels and low-

angle segments exploiting phyllosilicate-rich layers. Together with conjugated fractures, at the microscale we observe microcracks along foliation, we don't observe at mesoscale.
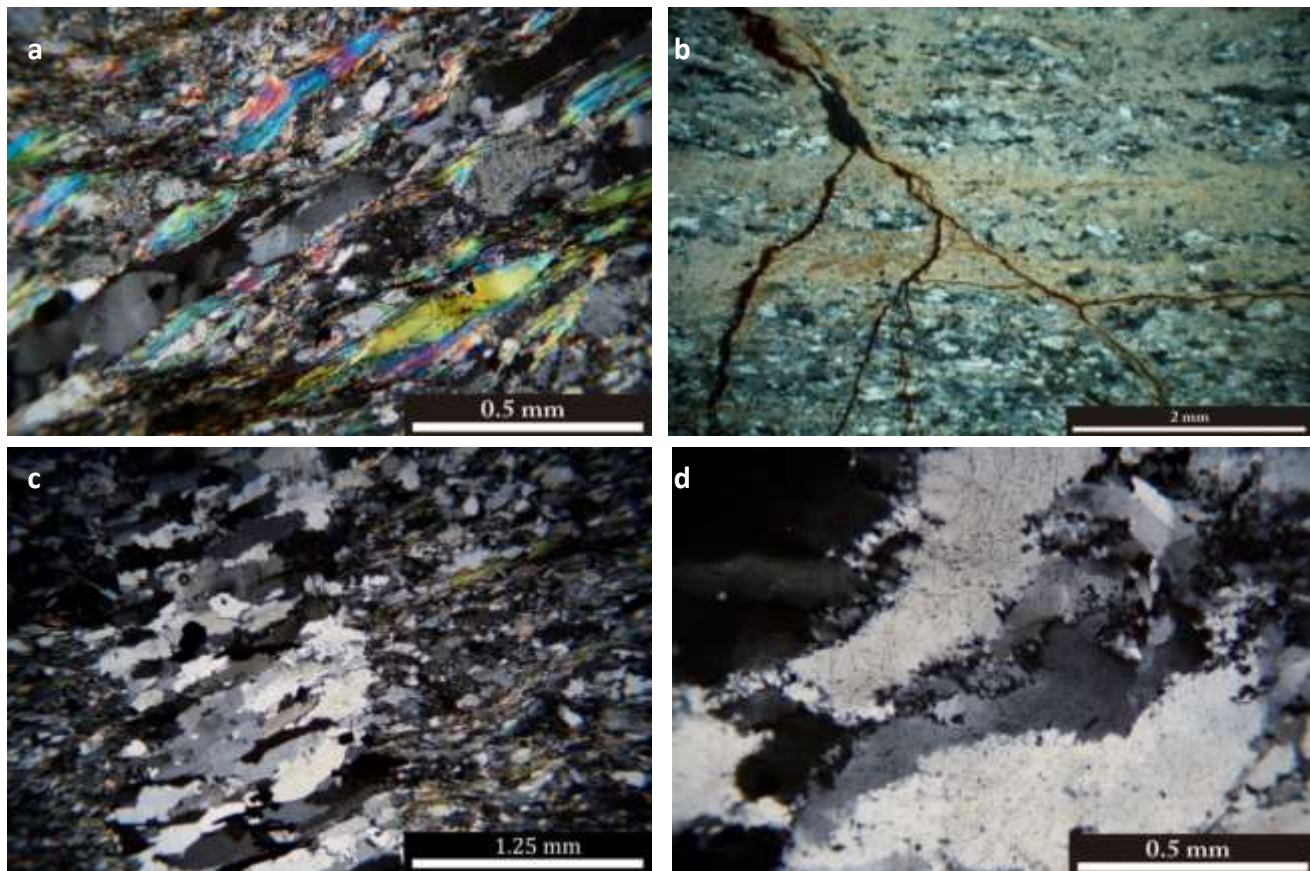

Figure 13 (a) Typical mineral assemblage , with the alternation of quartz and feldspar rich level and phyllosilicates rich level. (b)fractures both cutting foliation and along it. To notice fluid circulation with carbonate precipitation. (c) quartz vein. (d) low temperature recrystallization for bulging

2.6 Stress field reconstruction and slip tendency analysis

We reconstructed the paleostress field associated to the structures discussed in the previous sections - cataclastic layers along foliation, tensional joints and conjugated fractures - with Win-Tensor, a very flexible stress inversion package by Delvaux and Sperner (2003).

Stress inversion is in general based on the minimization of an objective function, which describes the distance between observable kinematic data and predictions based on a stress field model (Wallace 1951, Bott, 1959, Angelier and Mechler, 1977 and Angelier 1991). Win-Tensor implements different objective functions (hence its flexibility) and for this project we have used the F5 function (D. Delvaux and Sperner, 2003) that combines two contributions

$$F5 = [Term1 \times (1 - C.ratio)] + (Term2 \times C.ratio)$$

where *Term1* is the directional component given by the misfit angle (Angelier, 1977 and 1991) between the slip vector measured in the field and the tangential stress vector calculated by the model, and *Term2* expresses the attitude of a plane to slip by considering the resolved normal and shear stress; *C.ratio*, for which we used the default value of 0.05, balances the contribution of the two terms.

The best-fit stress field is characterized by σ1 and σ3 almost horizontal (Plunge/Trend 01/107 and 13/197 respectively), and σ2 almost vertical (Plunge/Trend 77/013), (Figure 14), suggesting a strike slip kinematics. The stress tensor shape factor shape factor δ = (σ2 - σ3) / (σ1 - σ3) is 0.6.

The misfit angle between observed and model slip vectors is on average 10°, pointing to a reliable solution. Win-Tensor also allows to test the stability of the solution with respect to rotations around the three principal stress axes (e.g. to test stability for rotation around σ1, σ1 is kept constant whilst σ2 and σ3 rotate around it). This is mainly defined by the orientation distribution of input data and our solution is rather stable for rotation around σ1 and σ2, but less stable for a rotation around σ3 (Figure 14).

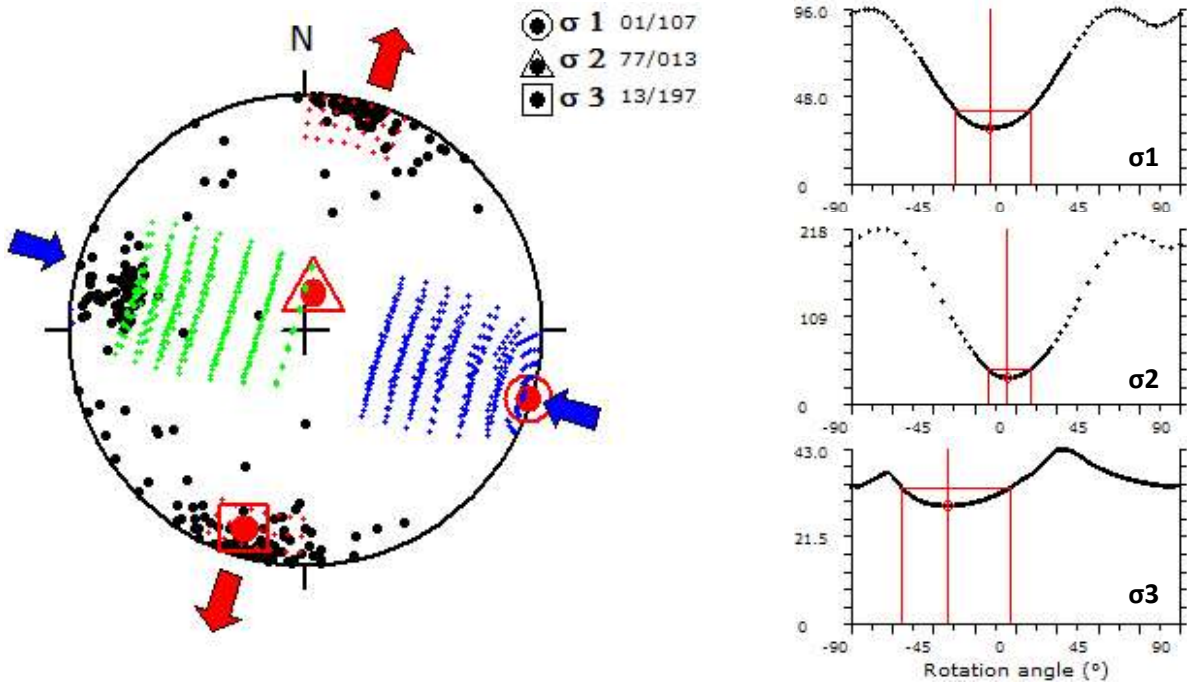**Figure 14 Reconstructed stress field: it show a strike slip kinematic with σ1 and σ3 almost horizontal and σ2 almost vertical. Green, red and blue strokes around axis represent their uncertainties we can observed also on the right, where we can observed the stability around σ1, σ2 and σ3**
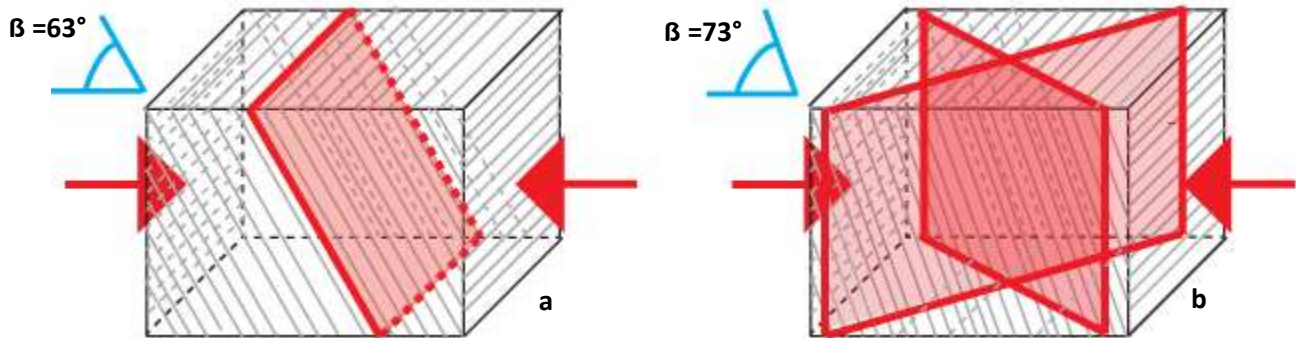

Figure 15 sketch of the two different behavior observe in the field: in (a), for ß = 63°, we observe brittle activation of foliation, in (b) instead, for ß = 73°, we observe the development of conjugated fracture planes.

Results of stress field inversion (σ1, σ2, σ3 orientation and δ = (σ2 - σ3) / (σ1 - σ3), have been used as input reduced stress tensor (Angelier, 1990) for slip tendency analysis. We calculated the normalized slip tendency:

$$NT_S = \frac{T_s}{\max(T_s)} = \frac{T_s}{\mu}$$

where T_s is the slip tendency define as $T_s = \frac{\tau}{\sigma_n}$, with $\boldsymbol{\tau}$ and $\boldsymbol{\sigma_n}$ tangential and normal stress respectively and $\max(T_s)$ is the maximum slip tendency. We calculated slip tendency for conjugated Andersonian fractures and for the three planes represented by the two average orientations of foliation (65/102, 75/102) and for intermediate value (70/102), hypothetically represented the transition between the development of conjugated fracture and foliation brittle activation. Figure 16a and 17c highlight the position of our brittle structures with respect to slip tendency values, projected both on Schmidt plt and on Mohr circles: Andersonian fractures are located in the maximum slip tendency area ($NT_s = 0.95$), whilst for the three other planes are in an area characterized by minimum slip tendency values ($0.20 < NT_s < 0.25$). Reactivated foliation planes show a value of slip tendency of 0.22, whilst the intermediate value of 70/102 $NT_s = 0.22$. These low values show how their activation is therefore unlikely in the isotropic case. Starting from slip tendency analysis, and by assuming 0.7 (Bayerlee, 1978) as internal friction coefficient (μ) for Andersonian fracture nucleation, we calculated μ for foliation activation: when foliation orientation is 65/102, $\mu = 0.14$, and when it dip 70°, $\mu = 0.154$ (Figure 16a and 16c). In Figure 16b and 16d we can observe Dilation Tendency (Td) analysis tensional which highlight the favourable orientation of field tensional joints, with a high $Td = 0.97$.

2.7   Discussion and conclusion

The Grandes Rousses massif rocks have been involved in three deformation events: the Hercynian and Alpine convergence and the Jurassic rifting. The last event – Alpine convergence - acted on rocks already characterized by penetrative pre-existing foliation.

Paleostress inversion allowed us to measure the relationships between the pre-existing foliation and principal stress axes associated to Alpine brittle deformation:

- tensional joints develop in the σ1/σ2 plane, with quartz and chlorite fibers growing parallel to σ3;

- conjugated fractures, which develop where foliation shows a dip anlge > 70°, have their intersection axis parallel to σ2 and the acute bisector parallel to σ1, so they can be interpreted as classical Andersonian fractures;

- brittle activation of foliation surfaces develops where foliation shows a dip angle < 70° (average Dip/Dip Azimuth 65°/102°);

If we define a ß angle as the angle between foliation and σ1, this is on average 73° in volumes characterized by Andersonian shear fractures and 63° in volumes characterized by cataclasite seams exploiting foliation. The limit ß angle defining the transition between the two deformation modes is 68° (Figure 16).

Mohr plot in Figure 16b highlights how for $ß < 68°$, slip along foliation is favoured, showing foliation planes weakness characterized by an internal friction coefficient of 0.154 (μ_{mis} for the limit value of $ß = 68°$), whilst for $ß > 68°$, the Andersonian behaviour is favoured and conjugated fractures develop, for their typical friction coefficient of 0.7 (μ_{And}). Anisotropy is quantifiable with the ratio μ_{mis} / μ_{And} that is 0.22, far from the isotropic value 1, and weakness along foliation planes is so important to partially influence Andersonian fractures too which develop a stairsteping morphology.

The behavior we observed in nature is very similar to the one observed in lab tests on the Four-miles gneiss by Kronenberg et al. (1990), where slip along cleavage is observed for an angle ß from ca. 20° up to c. 70°, and Andersonian fractures develop for higher ß (the transition at c. 70° in lab tests is corresponds to the 69° ß angle we deduced in nature). The control on brittle deformation modes in the Grandes Rousses micaschists and mylonitic gneiss is therefore two-face: (1) fracturing and slip along foliation induces an absolute weakness (Sibson, 1985), with a of friction coefficient of c. 0.154; (2) partial activation of [001] cleavage planes controls also the morphology of Andersonian fractures, which at the micro-scale show a stair-stepping geometry.
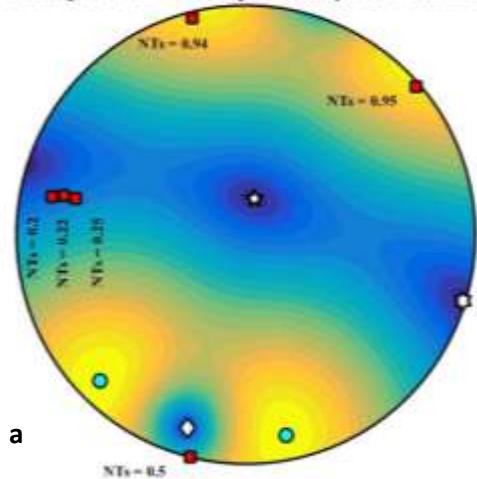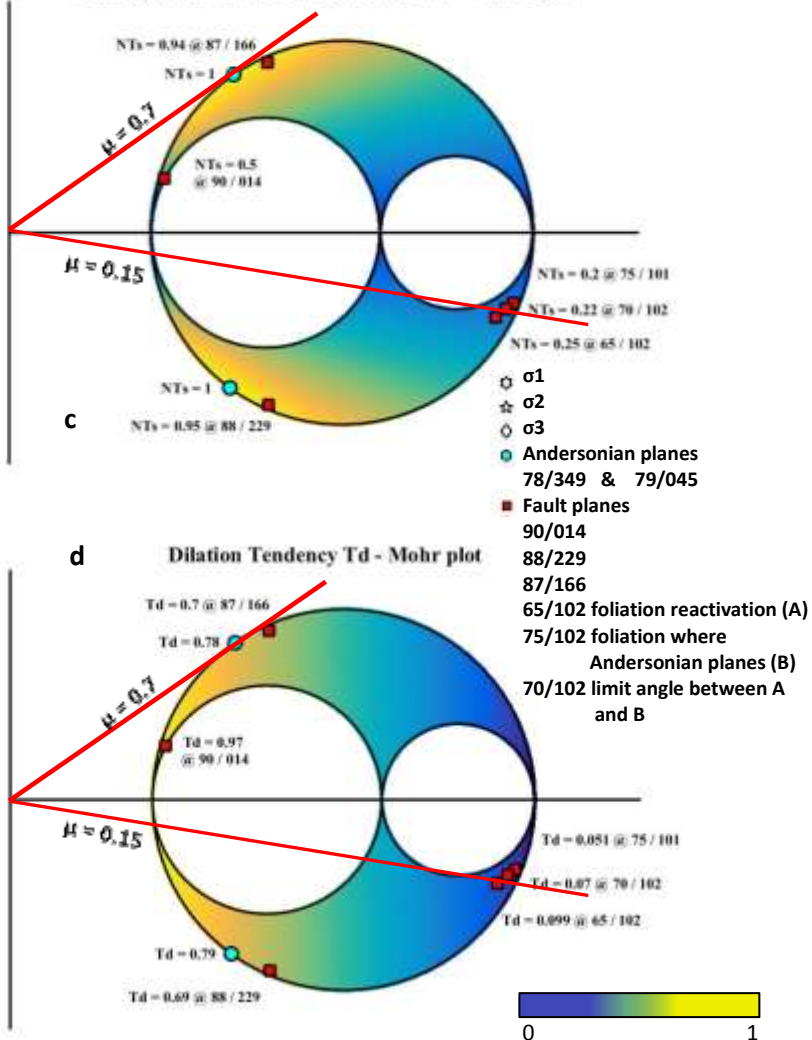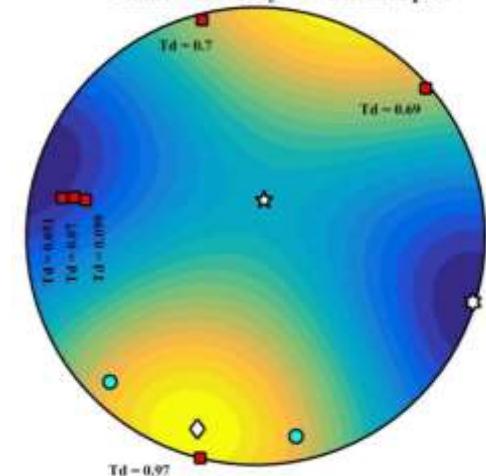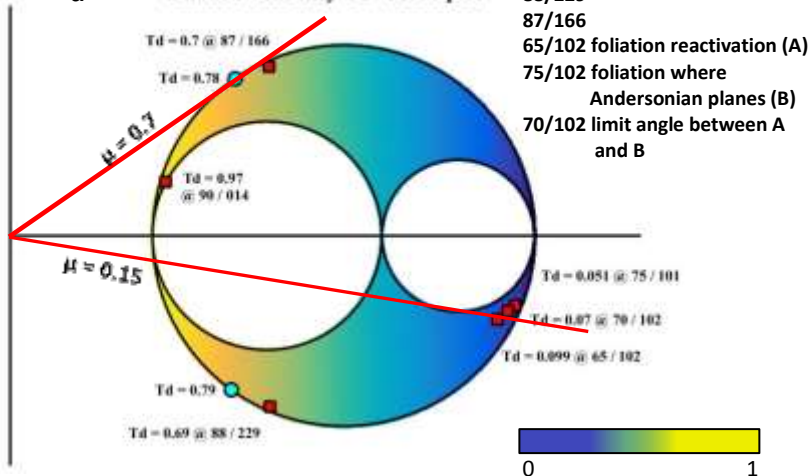
Figure 16 Slip Tendency analysis (NTs, in a and c) and Dilation Tendency (Td, in b and d). Projection of field data with respect to Slip Tendency (a) highlights misorientation of folation reactivated planes (NTs = 0.25) with respect to the Andersonian fractures (NTs =0.95). If we consider the T, foliation planes ctivation show always low values (<0.1). On the right , projection of NTs (c) and Td (d) on Mohr circles with in evidence our data position and failures envelopes for Andersonian fractures (μ=0.7) and the calculated μ for foliation reactivation of about 0.15.

2.8 Referencies

Angelier, J. 1991. Inversion directe et recherche 4-D: comparaison physique et mathematique de deux methodes de determination des tenseurs des paleocontraintes en tectonique de failles. Comptes Rendus de l'Academie des Sciences de Paris, 312(11), 1213-1218.

Angelier, J. & Mechler, P. 1977. Sur une methode graphique de recherche des contraintes principales egalement utilisable en tectonique et en seismologie : la methode des diedres droits. Bulletin de la Societe Geologique de France, 7(19), 1309-1318.

Attewell, P.B.&Sandford,M. R. 1974. Intrinsic shear strength of a brittle, anisotropic rock I: experimental and mechanical interpretation. International Journal of Rock Mechanics and Mining Science & Geomechanics Abstracts, 11, 423–430.

Barbier, R., Barféty, J.C., Bordet, P., Fabre, J., Petiteville, J., Rivoirard, R., Vatin-Pérignon, N., Mouterde, R., Méloux, J., 1977. Carte géologique de la France (1/50 000), feuille Saint Jean de Maurienne (774), Bureau de Recherches géologiques et minières, Orléans.

Barfety, J.C.,Gidon, M.,1983. - La stratigraphie et la structure de la couverture dauphinoise au Sud de Bourg d'Oisans. Leurs relations avec les déformations synsédimentaires jurassiques. Géologie alpine, t.59, p. 5-32

Bell, F.G. & Coulthard, J. M. 1997. A survey of some geotechnical properties of the Tees Laminated Clay of central Middlesbrough, North East England. Engineering Geology, 48, 117–133.

Bistacchi, A., Massironi, M., Menegon, L., Bolognesi, F., Donghi, V., 2012. On the nucleation of non-Andersonian faults along phyllosilicate-rich mylonite belts. Geol. Soc. London, Spec. Publ. 367, 185–199. doi:10.1144/SP367.13

Boriani, A., Dal Piaz, G. V., Hunziker, J.C., Von Raumer, J., Sassi, F.P., 1974. Caratteri, distribuzione ed età del metamorfismo prealpino nelle Alpi.

Bott, M.H.P., 1959. The mechanics of oblique slip faulting. Geological Magazine 96, 109–117.

Byerlee, J. D. 1978. Friction of rocks. Pure and Applied Geophysics, 116, 615–626.

Butler, R. W. H., Bond, C. E., Shipton, Z. K., Jones, R. R. & Casey, M. 2008. Fabric anisotropy controls faulting in the continental crust. Journal of the Geological Society, London, 165, 449–452.

Collettini, C., Niemeijer, A., Viti, C., Marone, C., 2009. Fault zone fabric and fault weakness. Nature 462, 907–10. doi:10.1038/nature08585

Collettini, C., Viti, C., Smith, S. a. F., Holdsworth, R.E., 2009. Development of interconnected talc networks and weakening of continental low-angle normal faults. Geology 37, 567–570. doi:10.1130/G25645A.1

Cox, S. F. 1995. Faulting processes at high fluid pressures: an example of fault–valve behaviour from the Wattle Gully Fault, Victoria, Australia. Journal of Geophysical Research, 100, 12 841–12 859.

Crouzet, C., Menard, G., and Rochette, P., 2001. Cooling history of the Dauphinoise Zone (Western Alps, France) deduced from the thermopaleomagnetic record: geodynamic implications. Tectonophysics, 340, 79-93.

Dal Piaz, G.V., Bistacchi, A., Massironi, M., Piaz, V.D., Geologia, D., Geofisica, P., Padova, U., 2003. Geological outline of the Alps. Episodes 26, 175–180.

Delvaux, D., Sperner, B., 2003. New aspects of tectonic stress inversion with reference to the TENSOR program, in: New Insights into Structural Interpretation and Modelling, Geological Society Special Publications. Geological Society, London, pp. 75–100.

Delvaux, D., Sperner, B., 2003. Stress tensor inversion from fault kinematic indicators and focal mechanism data: the TENSOR program, in: Nieuwland, D. (Ed.), New Insights into Structural Interpretation and Modelling, Geological Society Special Publications. London, pp. 75–100.

Donath, F. A. 1961. Experimental study of shear failure in anisotropic rocks. Geological Society of America Bulletin, 72, 985–990.

Donath, F. A. 1972. Effects of cohesion and granularity on deformational behavior of anisotropic rocks. Geological Society of America, Memoirs, 135, 95–128.

Dumont, T., Champagnac, J.-D., Crouzet, C., Rochat, P., 2008. Multistage shortening in the Dauphiné zone (French Alps): the record of Alpine collision and implications for pre-Alpine restoration. Swiss J. Geosci. 101, 89–110. doi:10.1007/s00015-008-1280-2

Durney, D.W., Ramsay, J.G., 1973. Incremental strains measured by syntectonic crystal growths. In: De Jong, K.A., Scholten, K. (Eds.), Gravity and Tectonics. Wiley, New York, pp. 67e96.

Duveau,G.,Shao, J.F.&Henry, J.P. 1998. Assessment of some failure criteria for strongly anisotropic materials. Mechanics of Cohesive-Frictional Materials, 3, 1–26.

Faulkner, D.R., Mitchell, T.M., Healy, D., Heap, M.J., 2006. Slip on "weak" faults by the rotation of regional stress in the fracture damage zone. Nature 444, 922–5. doi:10.1038/nature05353

Faulkner, D.R., Rutter, E.H., 2001. Can the maintenance of overpressured fluids in large strike-slip fault zones explain their apparent weakness? Geology 29, 503e506.

Ford, M. 1996: Kinematics and geometry of early Alpine, basement involved folds, SW Pelvoux Massif, SE France. Eclogae Geologicae Helvetiae 89, 269–295.

Gidon, M., 1979. Le rôle des étapes successives de déformation dans la tectonique alpine du Massif du Pelvoux (Alpes occidentales). Comptes Rendus de l'Academie des Sciences, 288, 803-806.

Gidon, M., 1999. L'origine des abrupts septentrionaux du Taillefer, massifs cristallins externes, Isère, France. Géologie Alpine, 75, 103-109.

Geology, S., Britain, G., 1993. Strength and anisotropy of foliated rocks with varied mica contents 15.

Hubbert, M. K. and Rubey, W. W. (1959): Role of fluid pressure in mechanics of overthrust faulting: I. Mechanics of fluid-filled porous solids and its application to overthrust faulting. Geol. Soc. Am. Bull., 70: 115-166

Kronenberg, A.K., Kirby, S.H., Pinkston, J., 1990. Basal slip and mechanical anisotropy of biotite. J. Geophys. Res. 95, 19257. doi:10.1029/JB095iB12p19257

McCabe, W. M. & Koerner, R. M. 1975. High pressure shear strength investigation of an anisotropic mica schist rock. International Journal of Rock Mechanics and Mining Science & Geomechanics Abstracts, 12, 219–228.

Morris, A., Ferril, A. & Henderson, D. B. 1996. Slip tendency analysis and fault reactivation. Geology, 24, 275–278.

Ramsay, J.G., 1980. The crack-seal mechanism of rock deformation. Nature 284, 135–139.

Rice, J.R., 1992. Fault stress states, pore pressure distributions, and the weakness of the San Andreas Fault, in: Wong, T. (Ed.), Fault Mechanics and Transport Properties of Rocks. Academic Press, pp. 475–503.

Sibson, R., 1981, A brief description of natural neighbor interpolation, in V. Barnett, ed., Interpreting Multivariate Data: John Wiley & Sons, 21–36.

Sibson, R.H., 1985. A note on fault reactivation. J. Struct. Geol. 7, 751–754. doi:10.1016/0191-8141(85)90150-6

Stipp, M., Stunitz, H., Heilbronner, R., Schmid, S. M. 2002: The eastern Tonale fault zone: 'natural laboratory' for crystal plastic deformation in quartz over a temperature range from 250 to 700°C. J. Struct. Geol. 24, 1861–1884

Townend, J., Zoback, M.D., 2004. Regional tectonic stress near the San Andreas fault in central and southern California. Geophysical Research Letters 31.

Twiss, R.J., Moores, E.M., 2006. Structural Geology, 2nd ed. W. H. Freeman.

Wallace, R.E., 1951. Geometry of shearing stress and relation to faulting. Journal of Geology 59, 118–130

Walsh, J. B. & Brace,W. F. 1964. A fracture criterion for brittle anisotropic rock. Journal of Geophysical Research, 69, 3449–3456.

Wernicke, B., 1981. Low-angle normal faults in the Basin and Range Province: nappe tectonics in an extending orogen. Nature 291, 645–648. doi:10.1038/291645a0

3 Brittle deformation of phyllosilicate-rich mylonites: failure modes and mechanical anisotropy

Francesca Bolognesi (a), Andrea Bistacchi (a) , Marcus Dobbs (b), Matthew Kirkham (b) & Sergio Vinciguerra (b, c, d)

(a) Department of Earth and Environmental Sciences, Università degli Studi di Milano Bicocca, Piazza della Scienza, 4, 20126, Milano, Italy.   E-mail: f.bolognesi1@campus.unimib.it.

(b) British Geological Survey, Environmental Science Centre, Nicker Hill ,Keyworth, Nottingham, NG12 5GG, UK

(c) Department of Geology, University of Leicester, University Road, Leicester LE1 7RH, UK

(d) Dipartimento di Scienze della Terra, Universita' di Torino, Via Valperga Caluso 35, 10125, Torino

3.1 Abstract

One mechanism explaining the nucleation and propagation of weak faults with non-Andersonian attitude is the mechanical anisotropy of phyllosilicate-rich mylonitic rocks. We characterized the mechanical anisotropy and (micro-)failure modes of phyllosilicate-rich (˂ 30%) mylonites from the Grandes Rousses Massif (Helvetic-Dauphinois Domain, French Alps). We performed 12 uniaxial (UCS) and 25 triaxial (TXT) tests varying the σ1/schistosity angle and confining pressures (0, 60 and 120MPa, and at a constant strain rate of 6*10-6 s-1. UCS at 90° show high strength and failure mode characterized by both low-angle segments along schistosity and high-angle ones cutting quartz-feldspar layers. UCS at 0° show lower strength and axial splitting along schistosity. TXT cover a complete range of inclinations, from 0° to 90°, at confining pressures of 60MPa and 120MPa. Maximum strength is achieved at 0°, strength and minimum strength, attained at 45°, is around 50% with a significant strength anisotropy. The "fault zone" develops mainly along schistosity for tests at 20-70°, whilst Andersonian shear fractures are observed at 0-20° and 70-90°. Microstructural observations reveal the dominant role of biotite foliation in the nucleation, propagation and coalescence of microcracking during dilatant failure. Foliated rocks is relevant in a wide range of σ1/schistosity angles and, due to failure modes dominated by along-schistosity slip, influences the angle to σ1 at which new macroscopic fault zones nucleate, which is very different from predictions of Anderson's theory.

3.2 Introduction

Phyllosilicates significantly influence the mechanical behavior of rocks (e.g.Collettini et al., 2009; Van Diggelen et al., 2010; Holdsworth et al., 2011). A literature review of laboratory tests have on foliated rocks been presented by Bistacchi et al. (2012), which considered experiments on slates (triaxial tests, Attewell & Sandford, 1974; Donath, 1961; Walsh & Brace, 1964), laminated clays (triaxial tests, Bell & Coulthard, 1997), phyllites (triaxial tests, Donath, 1972), chlorite and muscovite schists (triaxial tets, Duveau et al. 1998) and phyllonites (direct shear, Collettini et al., 2009). Literature show how tests on foliated rocks, with up to 25% phyllosilicates, mechanical anisotropy develops, as the internal friction coefficient (tangential stress/normal stress at failure) varies between 0.3 and 0.7 with respect to the orientations of the sample and the maximum compressive stress (,Bistacchi et al., 2012). This reflects different failure modes: when the foliation is favourably oriented, fractures develop along it and the rocks are weak, whilst when fractures cross the foliation at high angles, rocks are stronger (Jaeger et al., 2007). A foliated rock characterized by a (shape and crystallographic) preferred orientation of phyllosilicates is weak due to the weakness of (001) basal planes (Kronenberg et al., 1990), and theoretical studies show that the fraction of weak minerals needed to weaken a polymineralic rock is relatively small (e.g. Handy, 1990; Rawling, 2002), particularly if the phyllosilicates are organized in continuous films (e.g. Bistacchi et al., 2012).

The other important factor considered as weakening cause is the mechanical rock anisotropy, often easily identifiable with foliation.

The interaction between foliation, phyllosilicate content and weakening mechanism , has been discussed in (Bistacchi et al, 2012), with the description of three different representative geometries resulting from the interaction between stress field and foliation, by considering their mutual orientation. As we can see in Figure 17 (Bistacchi et al, 2012): in case (a) foliation I is approximatively perpendicular to σ1 and the rock behaves as an isotropic material, by developing Andersonian orientation fractures; in case (b) the angle between foliation and σ1(ß) is about 30°, and fracture planes develop with an Andersonian orientation along the foliation planes, but being driven from the foliation weakness and in fact failure happens for lower stress, because of the lower internal friction coefficient; in case (c) we can observe an example of "misoriented fault" with respect to the vertical σ1 and the relative angle formed with the
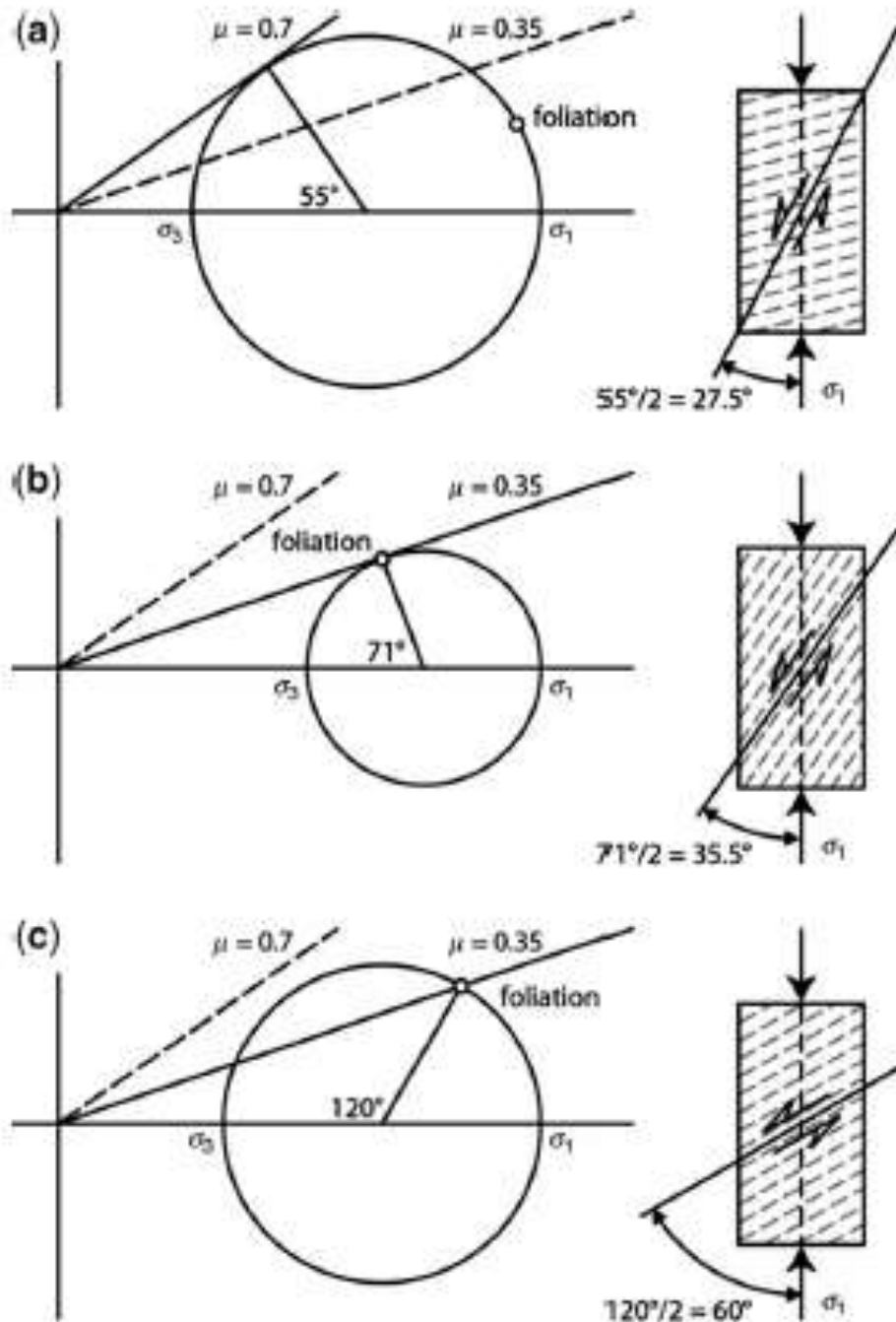
Figure 17 Different failure envelope for foliated rocks: (a) failure with Andersonian planes development; (b) failure along foliation witn an Andersonian orientation and law friction coefficient; (c) "misoriented" failure along foliation plane, with minor differential stress than case (a). more details inside the text. *(Bistacchi et al., 2012)*

foliation of 30° with the development of fractures along the foliation plane, whose activation results more favourable than Andersonian fault planes.

Phyllosilicate-rich rock mechanical properties have been discussed in literature and different models have been treated. Shea and Kronenberg (1993) describes three different deformation and failure modes in foliated rocks by considering (1) an unique plane of weakness represented by the foliation plane (Jaeger 1960, Donath 1961), (2) a continuously-varying anisotropy with respect to the angle between foliation and loading direction (Jaeger 1960, McLamore and Gray 1967) and finally (3) an isotropic response (Shea and Kronenberg, 1992).

Here we show the mechanical behavior of micashists from the Grandes Rousse Massif (French Alps), with a particular focus on the role of mechanical anisotropy, due to the highly foliated fabric and the phyllosilicates presence. After samples collection we run uniaxial compressive strength tests (UCS) and triaxial tests (TXT) during which the evolution of the microseismicity (Acoustic Emission (AE)), has been monitored too.

3.3   Investigated material

Investigated material is constituted by micaschists coming from the Groundes Rousses, on the French Alps. Before proceeding with mechanical tests, samples have been described and characterized for porosity and density values. In the selection of starting materials, we sought to minimize variations: regular foliation, absence of visible fractures, and absence of visible quartz veins, absence of folds. We selected in the field 16 blocks with a decimetric dimension. Main characteristic of these rocks is represented by thick foliation which locally develops a mylonitic fabric with the typical shear bands. Alternation of phyllosilicates and quartz and feldspar rich levels is thick, with a layer maximum thick of 500 μm and with an average grain size between 50μm and 200μm with a thin grain size. Fabric is the result of a complex deformation history: it is observable at microscale thanks to the presence of S/C/C' shear band, mainly marked by micas, and by the local precence of folds and microfractures. . By projecting the 2D microfractures orientation with respect to the foliation one, we can observe that microfractures are mainly concentrated along it, with a low deviation angle from foliation planes, but with little lateral continuity (Figure 18).

Thin sections images have been used also to estimate phyllosilicates content. We collected crossedpolar images with foliation trending at about 45° (Figure 19.) so that micas show higher interference colours with respect to other minerals.   Images were classified with a supervised maximum likelihood algorithm (e.g. Richards 1999) which, after a selection of training areas in the images, allows classified images to be generated with just three classes: phyllosilicates (red in Figure 19), quartz and feldspar (green in Figure 19) and not classified pixels (black in Figure 19). Phyllosilicates content has been estimated to be aroud 32% for a quartz and feldspar content of around 65% and a remained unclassified portion of 3%. This kind of analysis allowed us to visually estimate the interconnection of phyllosilicate layers, due to the strong shape-preferred orientation (SPO) of mica flakes and their organization in distinct and continuous layers (lepidoblastic fabric).

The characterization of the specimen physical properties, in terms of porosity and density has been effectuated following the ISRM standard. Both for specimen saturation and for submerged condition, the fluid used has been water. For each block, porosity and density have been measured from cores, after having drilled them. Number of measures for each block depends on core number we succeeded in drilling. In this way we have a punctual value for each single cylinder tested. Blocks show an almost constant density of about 2.75 g/cm3. On the other hand, porosity, show a higher variability, with low values ranging from 0.64 to 2.5, in agreement with presence of microfractures.
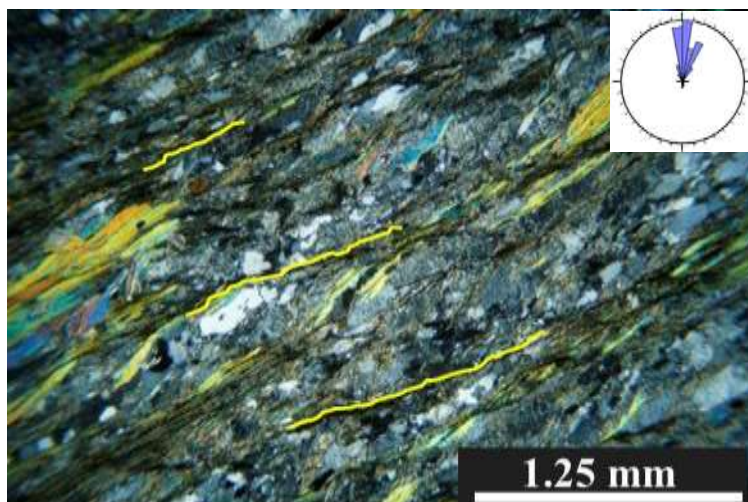
Figure 18 microfracture orientation with respect to foliation: in the plot North represents foliation orientation.

3.4 Rock deformation laboratory tests and physical properties evolution

Rock deformation laboratory tests and physical properties evolution has been tested at the Rock & Soil Physics Laboratory of the British Geological Survey in Keyworth, UK.

The experimental setup consists of a rock sample mounted inside a MTS 815 servo controlled stiff frame apparatus controlling the axial stress (σ1, UCS and TXT) and the radial confining pressure (σ3, TXT). Linear Variable Displacement Transducers (LVDT) applied on the sample consist of jaw axial strain extensometer and a chain-type circumferential strain extensometer. We carried out uniaxial compressive tests with no confinement and triaxial tests (TXT) with two different confining pressure, 60 MPa and 120 MPa. For some TXT tests Acoustic emission have been measured. Axial load has been applied at a servo-controlled strain rate of $6*10^{-6}$ s^{-1}.

Samples have been cored perpendicularly (x90°z) and parallelly (x0°z) to the foliation. TXT tests explored more directions in addition to the two main ones investigated throughout UCS tests, taking in account different orientations between 0° and 90°, formed by ß, the angle between foliation and σ1.
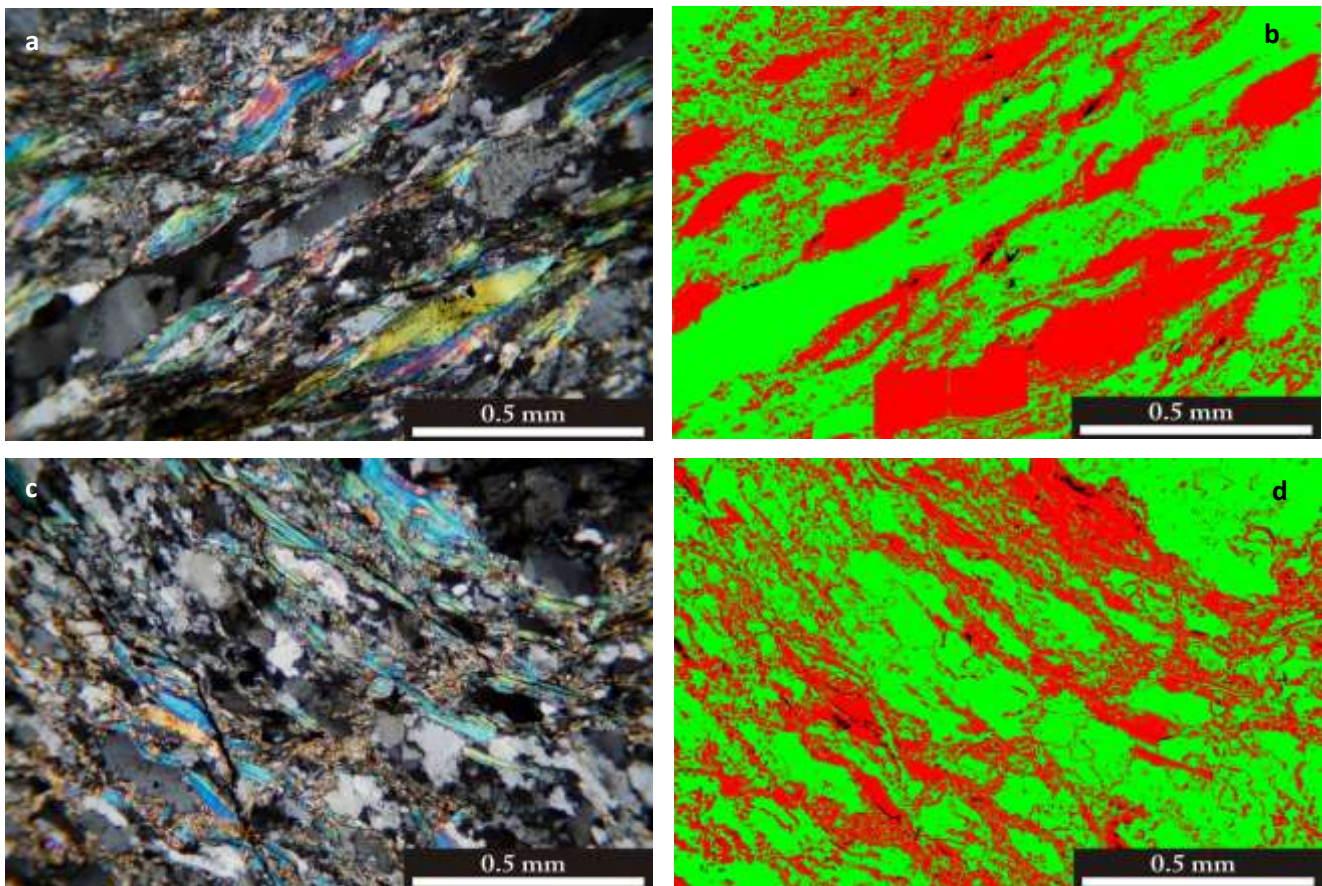
Figure 19 Image analysis with optical microscopy digital photos. (a, c) Colour photos of representative areas in thin sections (crossed polars). (b, d) Results of maximum likelihood image classification for (a) and (b), respectively. Red, phyllosilicates; green, quartz and feldspar; black, not classified pixels. Results of classification for the examples shown here: (a, b) phyllosilicates 39.8%, quartz and feldspar 58.6%, not classified 1.4%; (c, d) phyllosilicates 35.1%, quartz and feldspar 61.8%,

3.4.1 Sample preparation

We prepared cylindrical specimens for uniaxial compression tests (18 specimens, 37mm in diameter, 74mm in lenght) and triaxial compression tests (25 specimens, 54mm in diameter, 110-120mm in lenght). Specimens were trimmedand ground to ensure flatness and perpendicularity according to standard practices (ASTM D4543-04, 2004). UCS samples were cored from starting materials at 0° and 90 ° to their mesoscopic foliation, with the resulting sample orientations denoted x0°z and x90°z, respectively. TXT samples were cored from starting materials at different directions to their mesoscopic foliation, and have been gathered in three groups: i) x0°z tests, for samples loaded almost perpendicular to foliation, from 0° to 20°; ii) x90°z tests, for samples loaded almost parallel to foliation, from 70° to 90°; and iii) x45°z, for samples loaded along the intermediate orientations, 20° to 70°. TXT specimen have been surrounded by a teflon jacket to avoid the confining medium used, silicon oil, to permeate the sample during the test. Microcavities (1mm max) along cylinder surfaces have been filled up with some plaster, in order to prevent teflon jacket to fail under the confining pressure applied.

3.4.2 UCS tests

Uniaxial tests have been run on 20 testing two main directions: x0°z and x90°z, and for each direction we tested porosity from 0.8 to 2.5. In the following paragraphs we will describe the main characteristic of the two test types:

- x0°z tests: the failure strength observed in these samples falls between 32 and 83 MPa (Figure 20). The increase of the maximum strength mirrors the decreasing of porosity from ca. 0.8 to ca. 2.5 (Figure 22). Young modulus does not show a correlation with failure strength, and values vary between 27 and 56 whilst the Poisson ratio ranges from 0.08 to 0.42, with an average value of 0.28 (Figure 23). The analysis of the failure mode highlights the concentration of deformation along foliation planes with samples opening in axial splitting mode and the development of fractures along several planes (Figure 21). Image analysis of tested samples highlight the importance of foliation planes and phyllosilicates layers, with fractures developing mainly along [001] phyllosilicates level

or at the border between phyllosilicates and quartz and feldspar levels, where there is a mechanical contrast. .

- x90°z tests: the failure strength observed in these samples falsl between 50 and 117 MPa (Figure 20). As for the x0°z samples, the maximum strength increases mirrors the decreasing of sample porosity from ca. 0.8 to ca. 2.5 (Figure 22). Young's modulus (E) shows a perfect linear correlation with the maximum strength (a): E = 0.3382a - 4.2524 (R^2 = 0.9992). Poisson ratio varies from 0.09 to 0.25, with an average of 0.15 (Figure 23). Overall, the failure mode shows an Andersonian failure envelope with an angle of ca. 30° with respect to loading direction, but optical inspection highlights he steplike geometry of fractures, characterized by high angle millimetric microfracrures joint by horizontal microfractures following the foliation (Figure 21). Microfractures along foliation follow [001] mica planes whilst cutting foliation microfractures mainly cross and cross quartz and feldspar layers (Figure 21). Stress strain curves highlight a first non-elastic part, with a slow increasing in stress (Figure 20), suggesting the closure of microcracks along foliation during the first step of loading.

By considering the different porosity in samples, we calculated an anisotropy coefficient as the ratio between $\sigma_{x90°z}$ and $\sigma_{x0°z}$, which showed an average value of ca. 1.3 suggesting a different strength between the two main directions, with higher values for x90°z samples. Foliation control in UCS tests is therefore double, since foliation different orientation influences both sample strength, and failure mode by revealing its mechanical anisotropy.

3.4.3   TRIAXIAL test – Confining Pressure 60MPa

Triaxial tests have been run on 12 cores, 6 of them with AE collection. Here we describe the main characteristic of the three groups, x0°z, x90°z, and x45°z tests:

- x0°z tests: these samples reach failure strength for values of σ1 included between 261 and 303 MPa, and values of deviatoric stress included between 201 and 243 MPa (Figure 24). Poisson's ratio varies between 0.20 and 0.24 whilst Young's modulus show a greater variability, with values between 48 and 61 kN/mm^2 (Figure 23). The stress-strain curves highlight a peculiar behaviour in the segment between the yield point, at the end of the
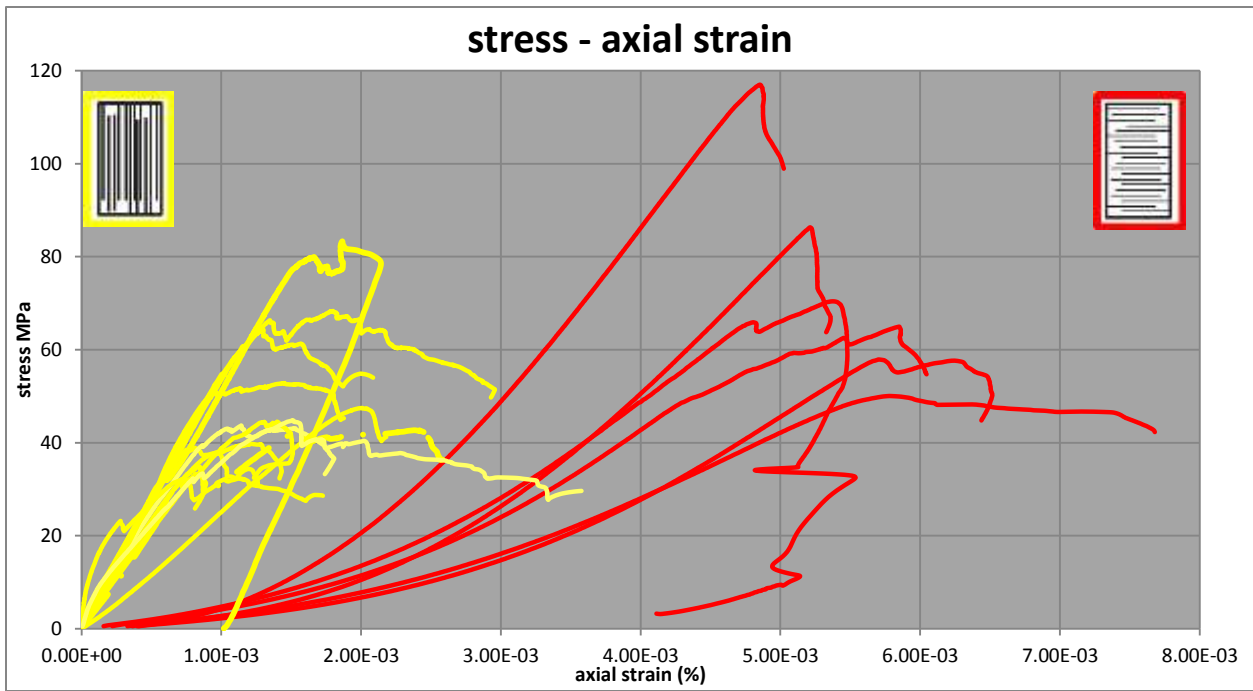
Figure 20 UCS stress-axial strain plot for the two loading directions: in yellow samples loaded parallel to foliation and in red samples loaded perpendicular to it. The two curve groups discern for stress peaks and for curve shapes.
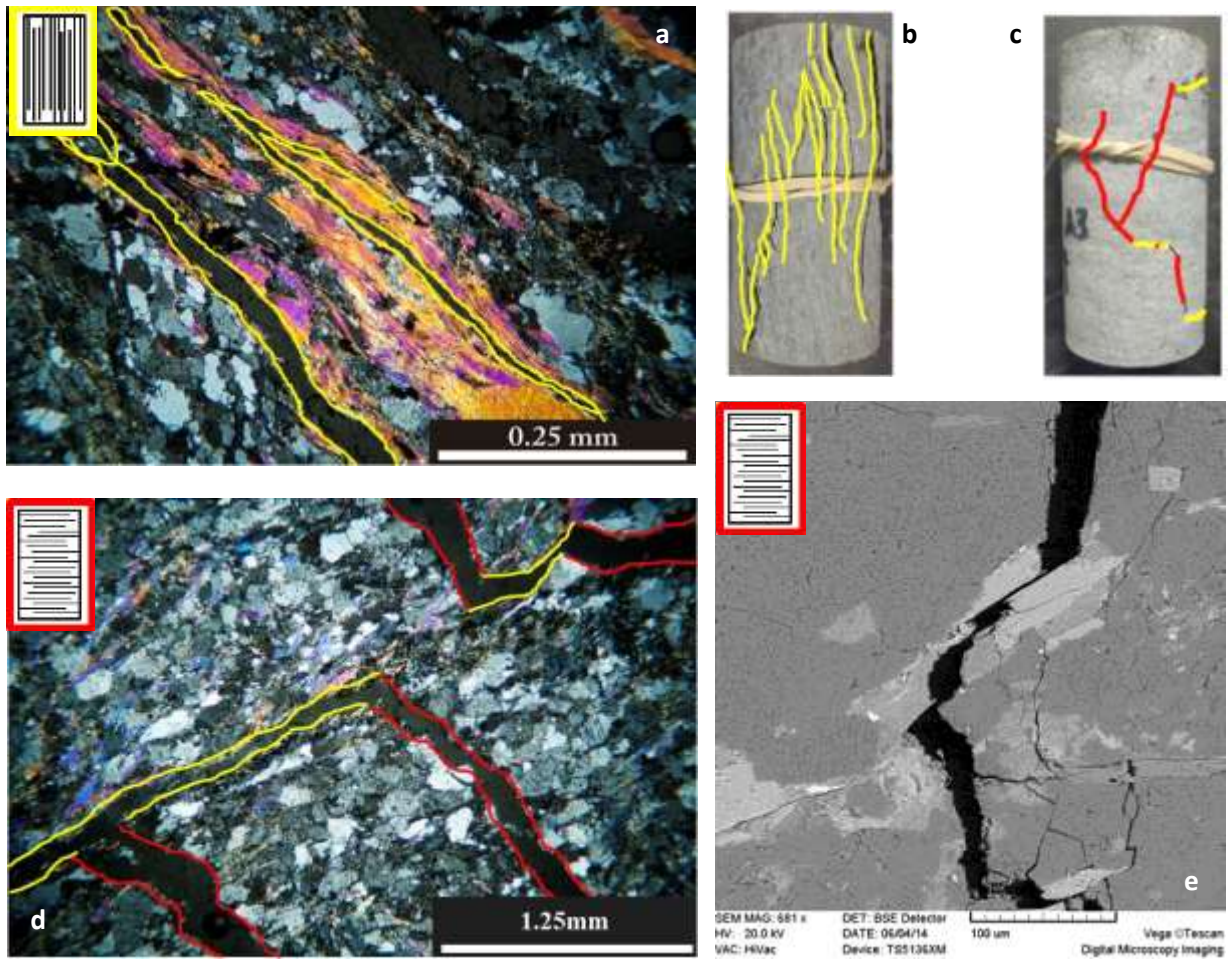

Figure 21 Post-UCS samples: in (a), (b) and (e): samples loaded parallel to foliation, with fracture exploiting foliation plane weakness and sample which opens and crashes in axial splitting; in (c), (d) and (e): samples loaded perpendicular to foliation and showing an Adersonian envelop of fractures characterized by a step-like geometry with segments cutting foliation (red) and segments along it (yellow). In (e) we can se the segment of fracture sliping along [001]mica planes, paralle to foliation, and the segment cutting it.

60

- elastic phase and the maximum strength, displaying the presence of several local and small peaks (Figure 28). The post peak curve, recorded until ca. 1% of total strain, show a sort of "plateau" for stress values really closed to the maximum: even if stress doesn't really increase, but swing around the maximum with a sequence of local peaks. AE are concentrated in the second part of the curve, with an increasing of both maximum average frequency from 600 kHz to 750 kHz and amplitude till a maximum of about 100dB (Figure 30). Samples after tests do not fail entirely, but reveal the presence of fractures concentrated along different foliation planes, in particular where foliation has higher folding with respect to σ1 direction. The optical analysis highlights the presence of deformation both along foliation and across it: along foliation fractures mainly follow phyllosilicate level weakness and [001] mica planes, with the development of open fractures with a lateral continuity of some millimetres. Fractures crossing foliation are less evident and are closed (Figure 26).
- x45°z tests: Failure is reached for values of σ1 included between 182 and 256 MPa and values of the deviatoric stress included between 122 and 196 MPa (Figure 24). An almost constant Poisson ratio, ranging from 0.25 to 0.30, and a Young's modulus varying from 27 to 55 kN/mm^2 is found, with a positive correlation with the increasing in maximum strength (Figure 23). The analysis of stress-strain curves shows the presence of small stress drops in the pre-peak part of the curves. The failure peak is evident only in samples with an angle of 65° and 68° between σ1 and foliation, that after the peak, shows a decreasing in loading and it reaches a residual stress value. For the other loading directions (20°, 30° and 45°) the maximum strength does not correspond to a real peak but to the achievement of a steady state represented by the typical "plateau" in the curve shape, with stress oscillation around the maximum corresponding to a continuous strain increasing. AE analysis shows a really low presence of emissions throughout the tests, with an increasing after the yield point, but with a really low total number of less than a thousand of AE which show a low frequency with maximum at about 600 kHz and a concentration around low frequency (<450 kHz) (Figure 30).

The failure mode we observed in samples, is always a deformation following the weakness of foliation planes, with their activation for all the orientation ranges of this group, which is the only deformation observable in thin sections (Figure 25)

- x90°z tests: Failure is reached for values of σ1 included between 268 and 276 MPa, with the values of deviatoric stress included between 208 and 216 MPa (Figure 24). Elastic moduli are quiet constant, with a Poisson's ratio of 0.24 and a Young's modulus of about 43 kN/mm^2 (Figure 23). Stress-strain curves are quiet linear until the maximum, which is followed by a quiet low decreasing. Samples don't develop a real failure plane, but they look relatively intact, with slip planes visible along foliation and across it with a stair step geometry, with an envelope Andersonian orientation (Figure 27). AE analysis highlights a progressive increasing in AE rate during all test: we observe maximum frequency at about 800kHz with a significant increasing in low frequency emissions in the last part of the TXT curve, characterized by low slope and associated to the formation of bigger fracturing sources (Figure 30).

Overall, for TXT tests, with a confining pressure of 60 MPa, as for UCS tests, we calculated an anisotropy coefficient on the deviatoric stress, as the ratio between $\sigma_{x90°z}$ and $\sigma_{x0°z}$ of 0.96 and another value of anisotropy between $\sigma_{x90°z}$ and $\sigma_{x45°z}$, as used in Shea and Kronenberg (1993) of 1.61: This imples that there is not a real difference in peak strength between the two main loading directions. However the difference with the minimum peak strength, with an orientation around 45°, it is significant.
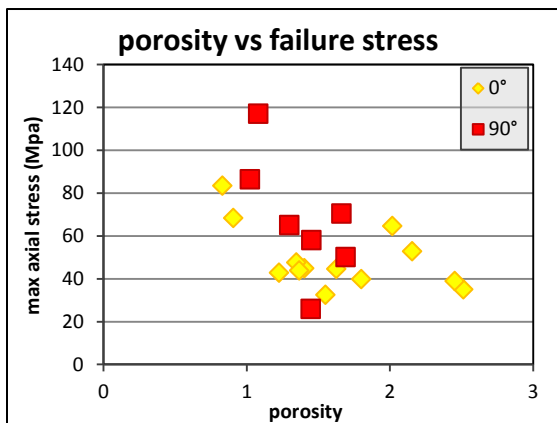
Figure 22 Negative correlation between maximum axial stress and porosity in UCS
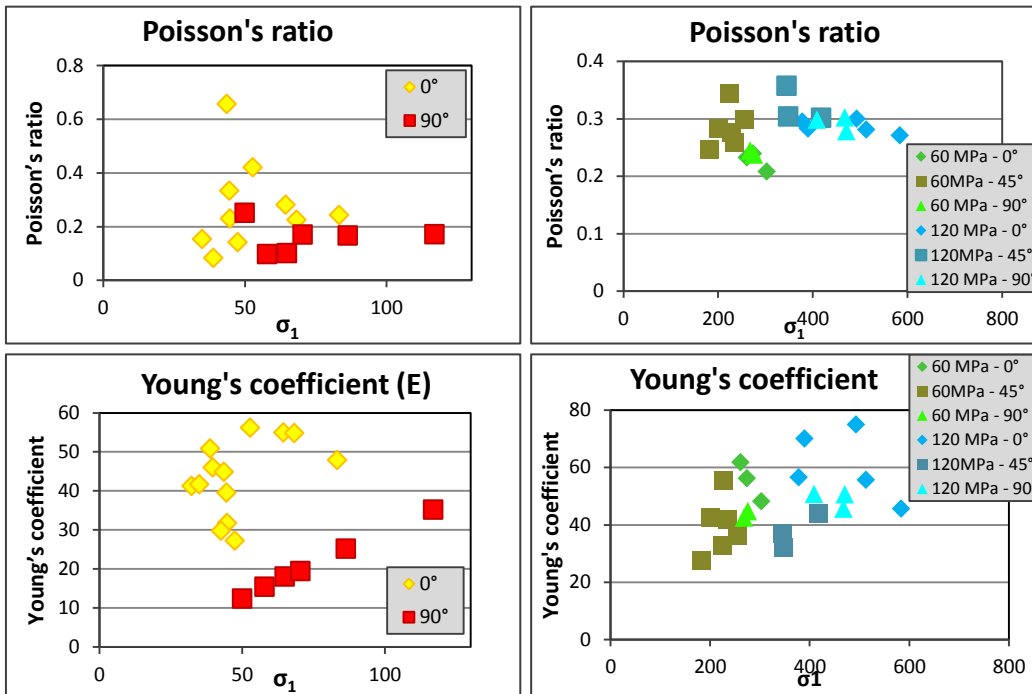
Figure 23 Young's coefficient and Poisson's ratio for both UCS (on the left) and TXT tests: young's coefficients show a positive correlation with respect to σ_1. Poisson's ratios don't show any correlation with σ_1. Both values increase from UCS tests and TXT tests

3.4.4 TRIAXIAL test – Confining Pressure 120MPa

Triaxial tests have been run on 13 cores, 6 of them with AE collection. Here we describe the main characteristic of the three groups, x0°z, x90°z, and x45°z tests:

- x0°z tests: these samples reach the failure strength for values of σ1 included between 378MPa, for an angle of 20° with foliation and 584 MPa, for an angle of 20° with foliation and values of the corresponding deviatoric stress included between 258 and 393 MPa (Figure 24). Poisson's ratio is quiet constant and varies between 0.27 and 0.30 whilst Young's modulus show an higher variability, with values between 55 and 74 kN/mm^2 (Figure 23). Therefore samples show a more ductile behavior, since the deformation is less localised. This is evident in Stress-Strain curves too, which don't show a sharp peak, but, after the elastic behavior, a gradual increasing until a maximum value of strain, followed by a slow decreasing recorded until more than 1% of strain,
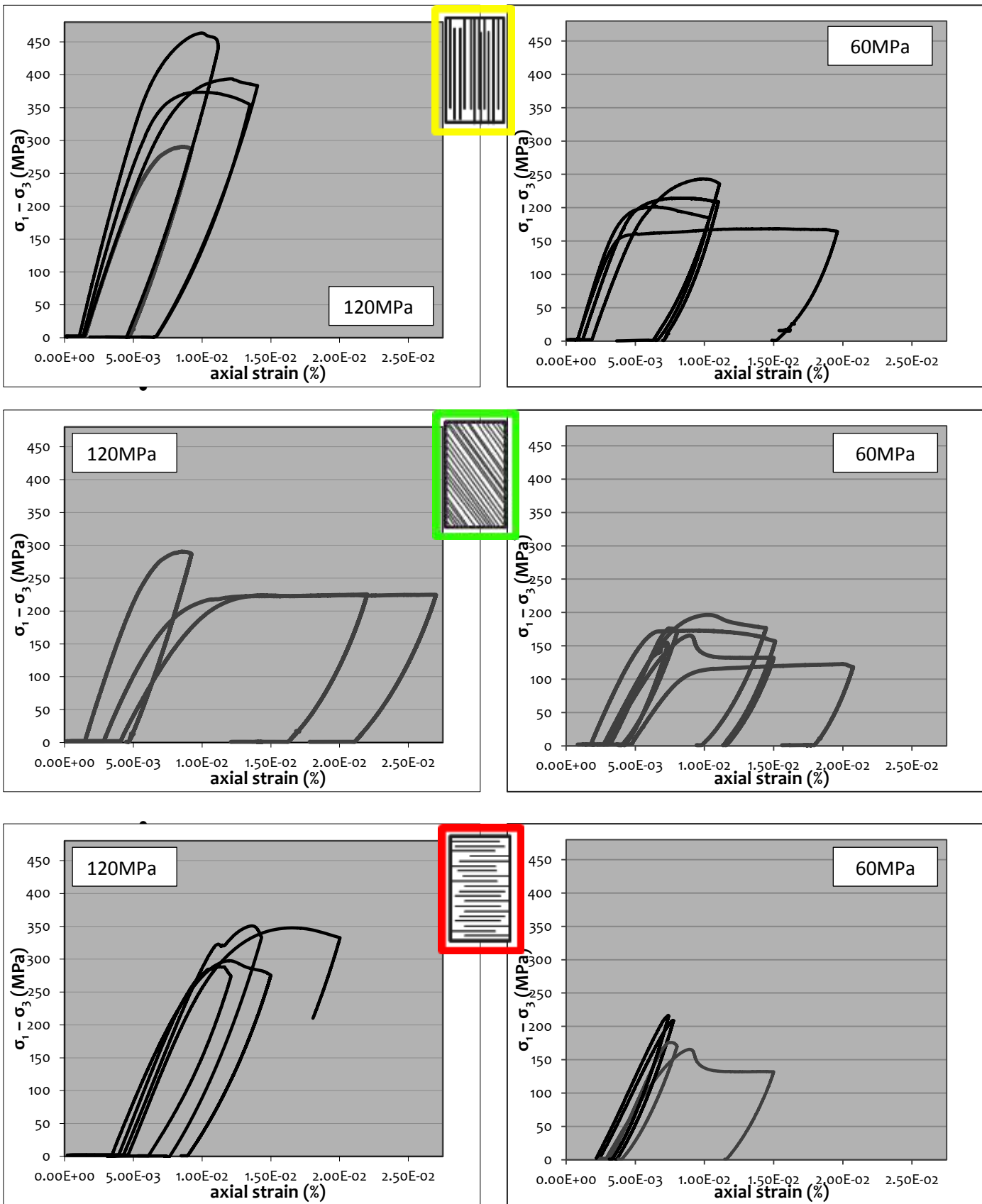
Figure 24 Relationship between differential stress (σ1 – σ3) and axial strain for TXT tests for the three groups : at the top, 0°<ß<20° ; in the middle 20°<ß<70° and at the bottom 20°<ß<70°. On the left, samples have been tested with a confining pressure (Pc) of 120MPa, on the right Pc=60MPa
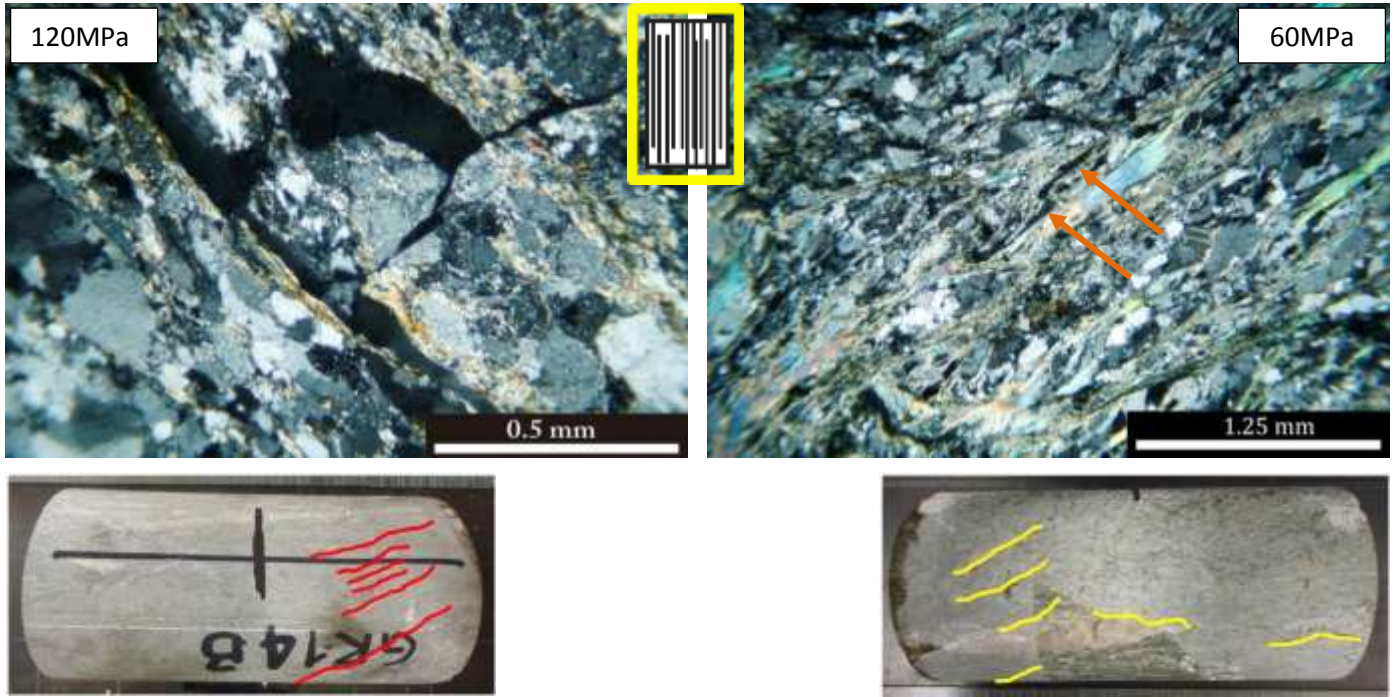
Figure 25 Failure modes for sample loaded with 0°<ß<20°: for both confining pressure stair-step fractures develop
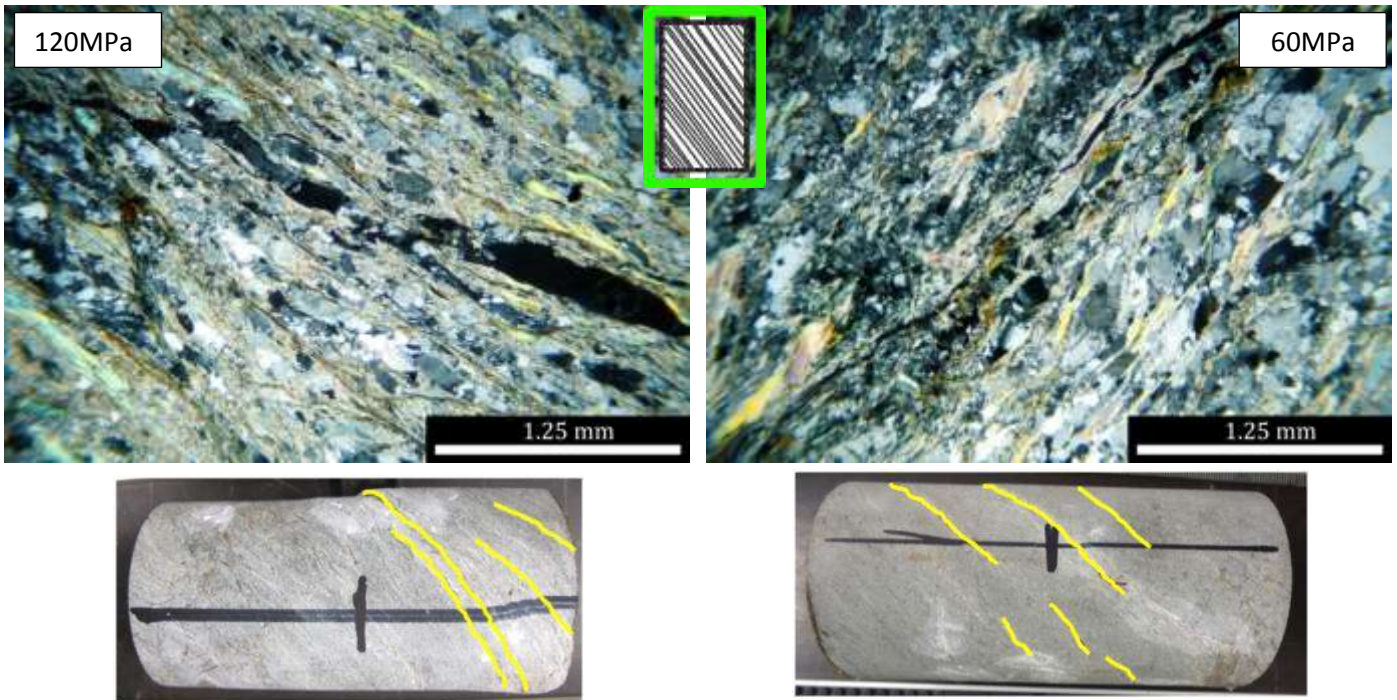
Figure 26 Failure modes for sample loaded with 20°<ß<70°: for both confining pressure samples show slipping along foliation planes with the activation of more foliation planes
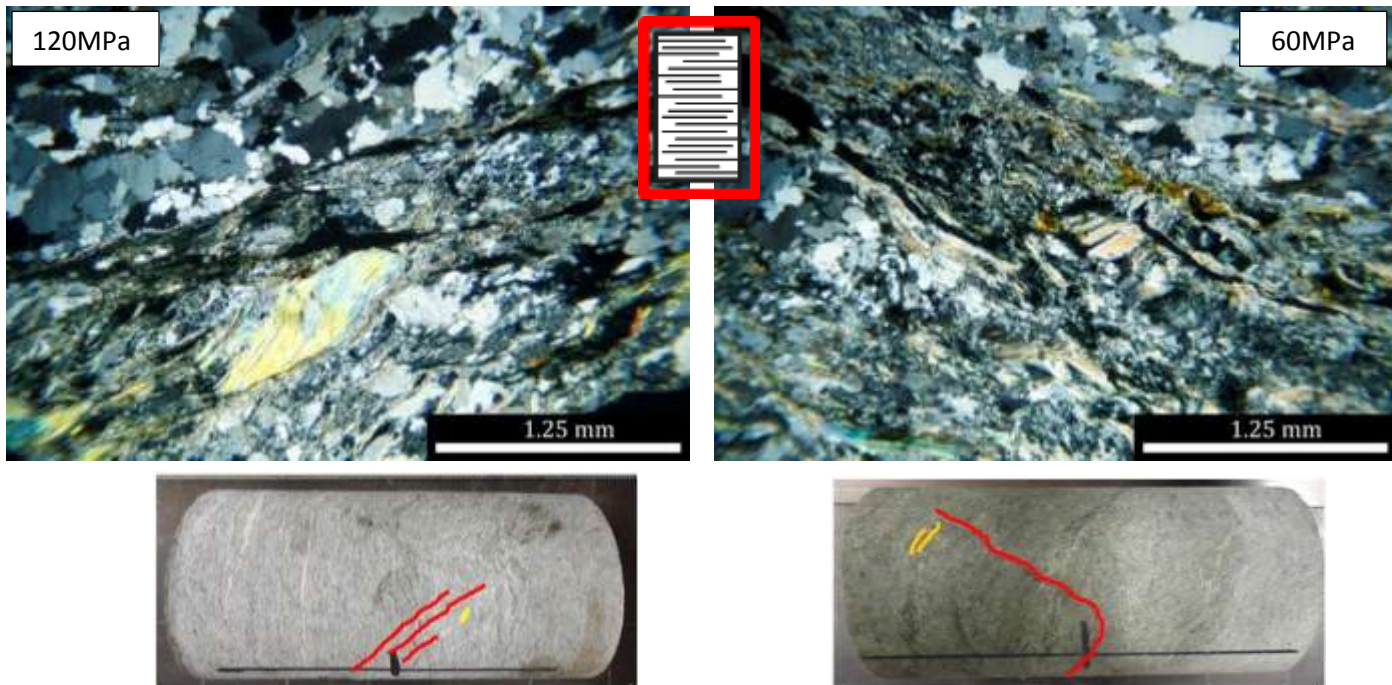
Figure 27 Failure modes for sample loaded with 70°<ß<90°: for both confining pressure stair-step fractures develop with an Andersonian orientation

- when the test was stopped. AE are concentrated in the second part of the curve, the more "ductile", with a maximum average frequency of 800 kHz and maximum amplitude of about 100dBAE (Figure 30). Thin sections highlight the presence of rare fractures developed both along foliation, along phyllosilicate levels, and cutting it, through quartz and feldspar levels, with a stair step geometry (Figure 25).

- x45°z tests: failure is reached for values of σ1 going from 345MPa (deviatoric stress 225MPa), for an angle of 45°, and 418 MPa (deviatoric stress 298 MPa), for an angle with foliation of 70°, and passing throw a peak of 415MPa (deviatoric stress 295MPa) for an angle of 24°. This variation shows how the different inclinations, from 20° to 70°, switch from an higher strength for the end member foliation orientation (24° and 70°) to a weaker behavior for an intermediate orientation (45°) . Stress-strain curves highlight a variability in Poisson's ratio, from 0.25 to 0.36, and a Young's modulus varying from 31 to 57 kN/mm^2, with a negative correlation with the increasing in σ1 (Figure 23). The

failure mode is always driven from a major fracture following the weakness of foliation planes, with slip along more planes overlapping each other. These behaviors can be identified not only by eye's inspection, but also throughout the deformation curves, characterized by the presence of small peaks followed by a new increasing in loading (Figure 26). Similarly to 60MPa x45°z tests, AE, which are less numerous with respect to the other orientations, show a concentration after the yield point of Stress-Strain curve and a concentration of frequency at a low value, of about 600kHz related to major fractures formation (Figure 30)

- x90°z tests: Failure is reached for almost constant values of σ1 ranging between 409 and 468 MPa, with the values of deviatoric stress included between 289 and 351 MPa (Figure 24). Here, elastic moduli are quiet repeatable, with a Poisson's ratio of 0.30 and a Young's modulus ranging between 45 and 50 kN/mm^2 (Figure 23). Similar failure peaks and elastic moduli are found with a measured angle of foliation between 80° and 85°. Samples do not fail completely, but we can observe sets of fractures developing with an high angle with respect to the foliation, with the typical Andersonian orientation and an angle with σ1 of about 30°. Fractures are not linear but they show a 'stair' step like geometry with the alternation of segments following the weakness of foliation planes and segments cutting quartz and feldspar levels. Here AE are concentrated in the elastic part of the curve (Figure 30), showing a decrease in number and average frequency in the ductile regime, probably linked to the linkage of more cracks.

Overall, for TXT tests, with a confining pressure of 120 MPa, as for previous tests, we calculated an anisotropy coefficient, as the ratio between $\sigma_{x90°z}$ and $\sigma_{x0°z}$ of 0.94 and another value of anisotropy between $\sigma_{x90°z}$ and $\sigma_{x45°z}$, as used in Shea and Kronenberg (1993) of 1.76. With respect the TXT tests at 60MPa confining pressure, A significant difference in peak strength between the two main loading directions is not observed, but the ratio with the minimum peak strength, with an orientation around 45°, is important with a value close to 2 and showing an increment in anisotropy between these two directions with respect to the 60MPa confining pressure tests.

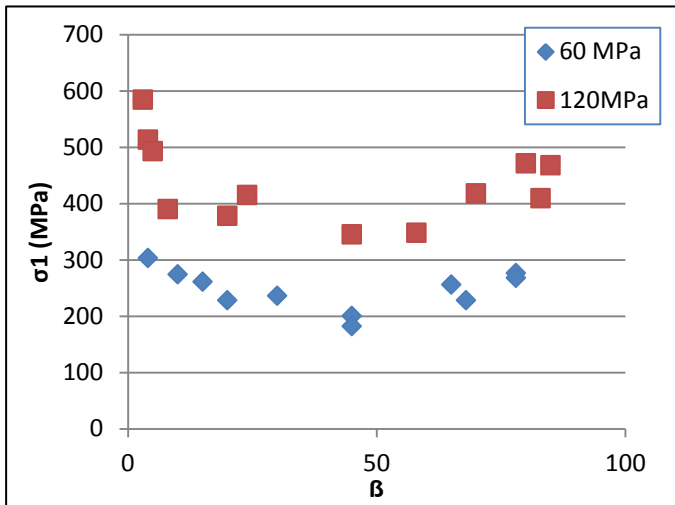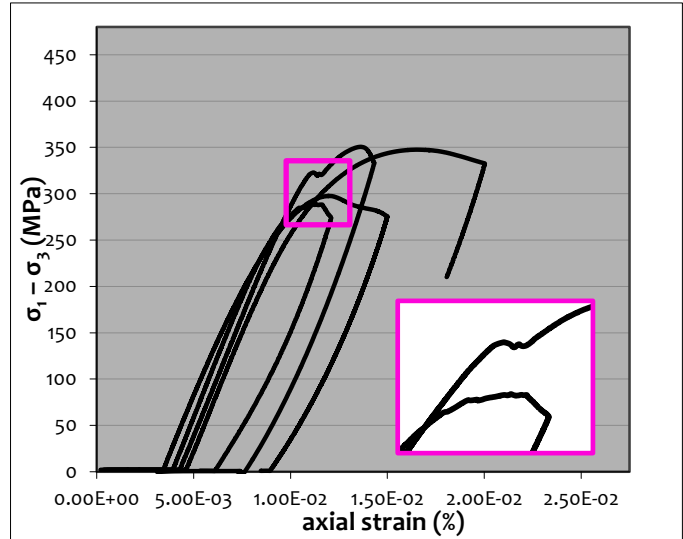**Figure 28 local peacks in TXT tests ascribable to a "stick-slip" behaviour**

Figure 29 Projection of maximum compressive stress σ1 with respect to angle between σ1 and foliation orientation for the two confining pressure: "U" curve shape highlight a wide weakness intervall

3.5 Discussion and conclusions

Grandes Rousses micashists are rocks characterized by an high angle foliation where phyllosilicates, whose content is about 30%, show a neat preferred orientation and are organized in continuous layers. The mechanical characterization through UCS and TXT highlighted the different mechanical behaviour with respect to the different confining pressures applied and different loading directions with respect to the foliation. Confining pressures applied at 60 and 120 MPa induced a different anisotropy ratio if we consider the two main directions, with ß = 90° and ß = 0°: in fact the ratio σx90°z and σx0°z is 1.3 for UCS tests, suggesting an higher strength for samples tested at 90°, whilst this difference in TXT seems to disappear with values of 0.96 (60MPa) and 0.94 (120MPa) which highlighted a substantial

68

equivalence between the two directions, until a weak strength inversion for the two directions. When considering TXT halfway direction tests, relationship ß/strength ratio highlight a continuously-varying anisotropy (Jaeger 1960, McLamore and Gray 1967) with the two end-member directions, x0°z and x90°z showing the maximum strength, whilst for all the other directions a weaker behaviour is found with a minimum at 45°. The two curves stress/strength (Figure 29) for the two different confining pressure, 60MPa and 120MPa show a comparable pattern, but with higher strength values at 120MPa, as expected. The anisotropy ratio, calculated as the ratio between the strength measured along the two directions given by ß~90° and ß~45° (minimum), is 1.61 and 1.76 for 60MPa and 120MPa respectively, in agreement with the values found in Shea and Kronenberg (1993) for schist and gneiss lithologies.

UCS have shown in a clear way the two different failure modes: samples loaded parallelly to the foliation develop fracture opening along foliation planes (axial splitting) (Figure 21c-d), whilst specimens loaded perpendicularly to the foliation record an high angle failure envelope, with an Andersonian orientation, but constituted by high angle millimetric microfractures crossed by microfractures horizontally distributed along foliation, which generate a 'stair' steps geometry (Figure 21fa-b).

The different failure modes evidence a widespread foliation control. For the x0°z and x90°z tested samples, fracture envelops orientation may be considered "Andersonian", but their step-like geometry, due to the brittle rupture of some bits of the foliation, evidences its intrinsic weakness, even when foliation surfaces are not favourably oriented. Acoustic emissions are mainly concentrated after the yield point and correspond to distributed damage accompanying the cracks coalescence and growth . For sample group x45°z, the foliation weakening behaviour is clear and can be observed throughout the slip along more foliation planes. For x0°z and x90°z samples, AE are again occurring mainly after the yield point, but they are characterized by lower frequency and a lower total number. Foliation and mica control in brittle behaviour of Grandes Rousses micashist is therefore double fold: (1) a favourable foliation orientation (20°<ß<70°) implies a lower mechanical strength, and so a weak behaviour; (2) brittle activation (or partially brittle activation) of foliation surfaces and [001] mica planes have a fracture like

control both in weak samples (20°<ß<70°) and in samples characterized by the development of Andersonian fractures, which show a stair-step geometry.

Figure 30 Follow diagram show an example for each direction group tested and for the two confining pressure of AE data: we plotted together data of differential stress, amplitude, frequency, hit's cumulative and AE hit's rate.

■ AE Hit's rate
■ Hits Cumulative (/100)
■ Frequency
■ Amplitude
■ Differential Stress (σ3-σ1)

90° - 120MPa

90° - 60MPa

45° - 120MPa

45° - 60MPa

72
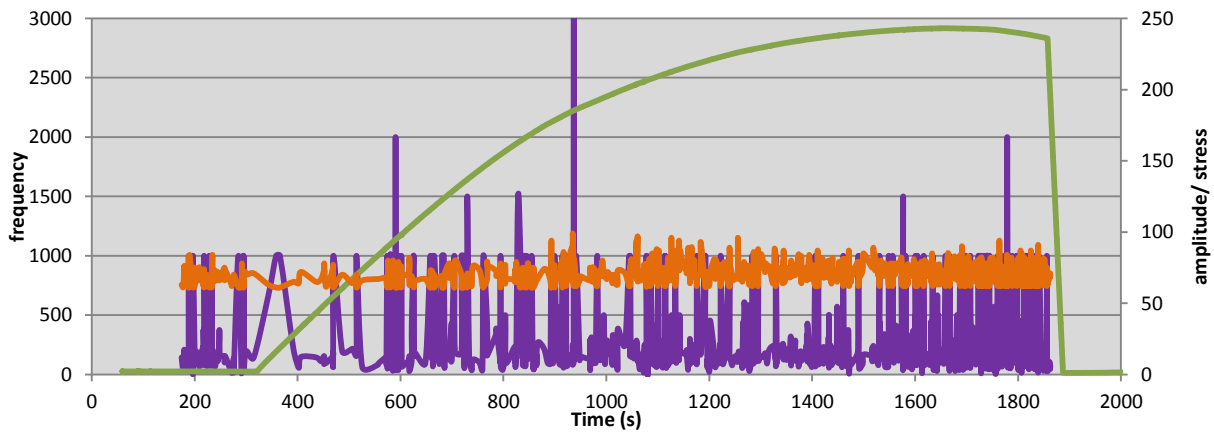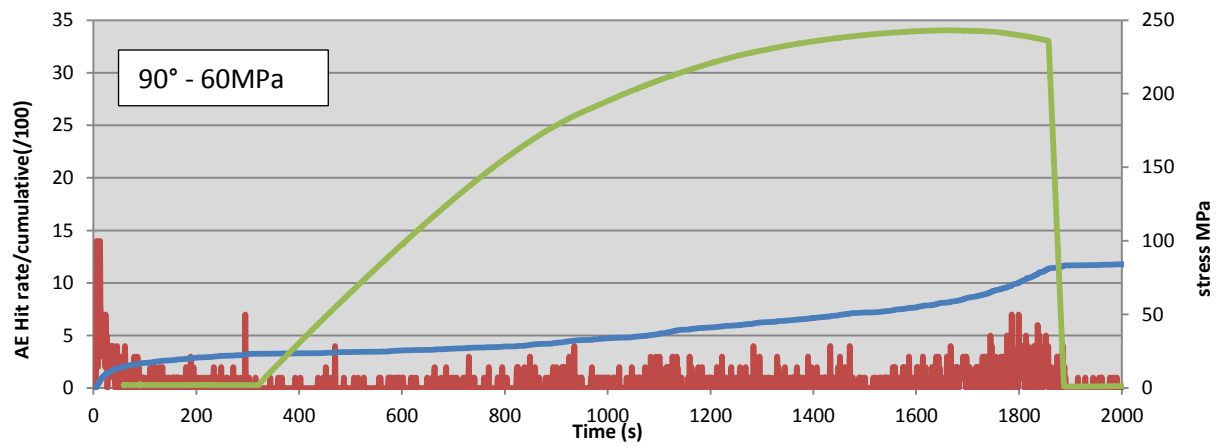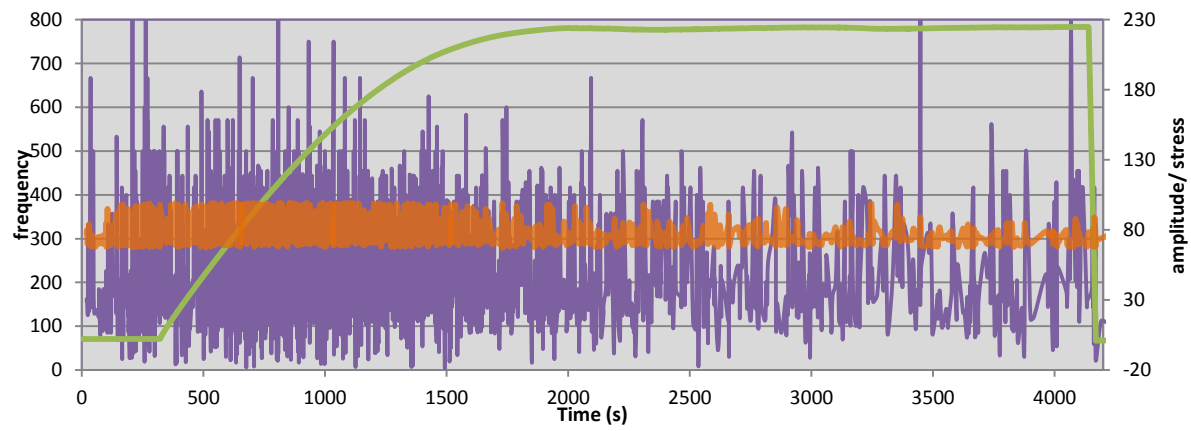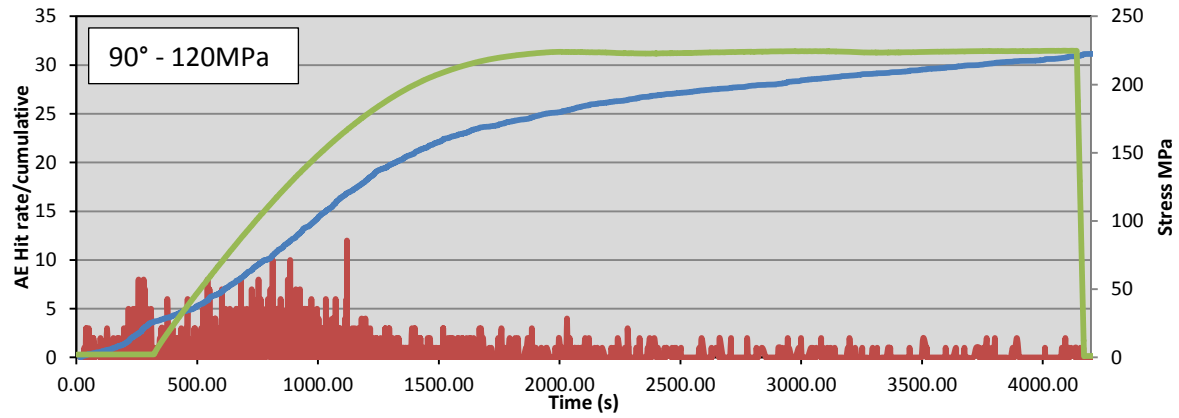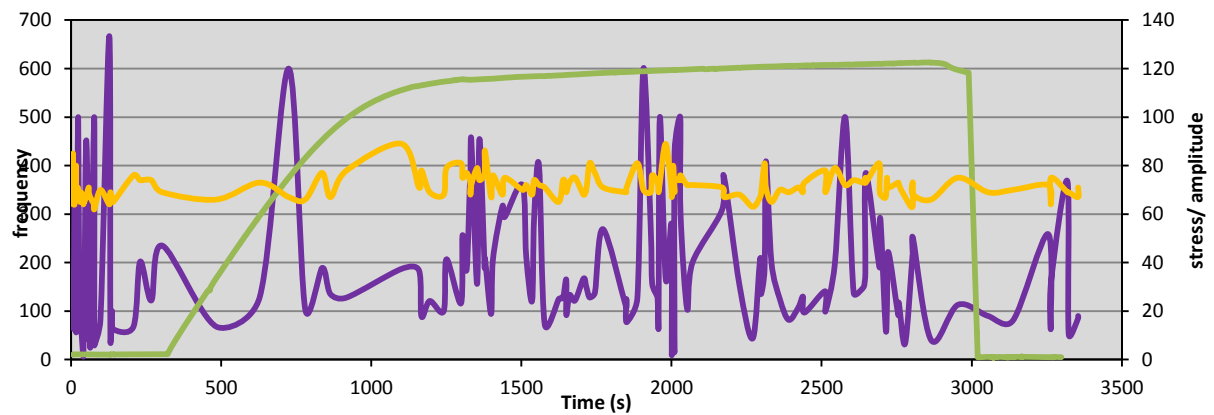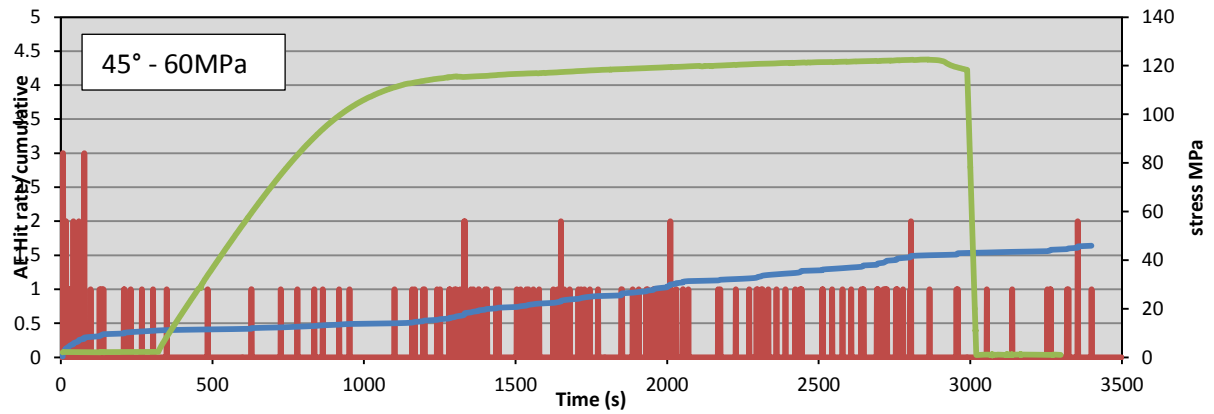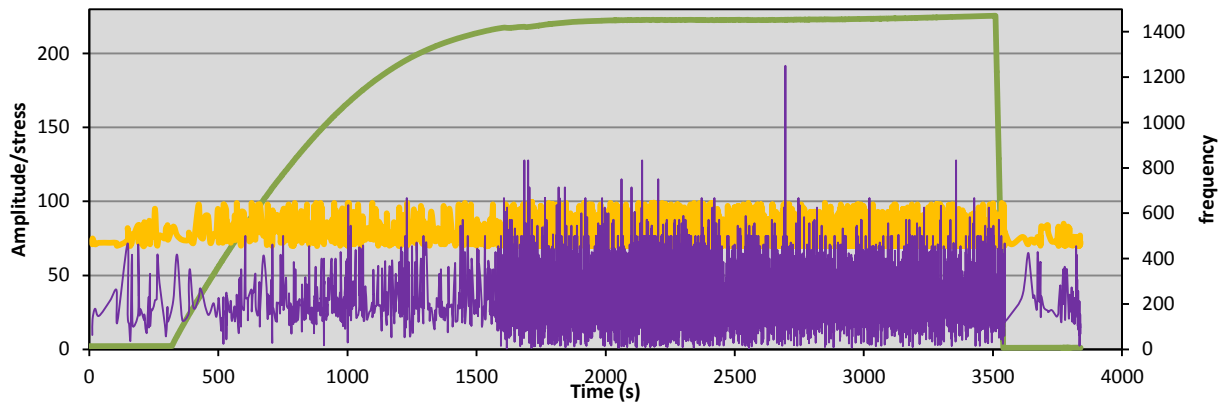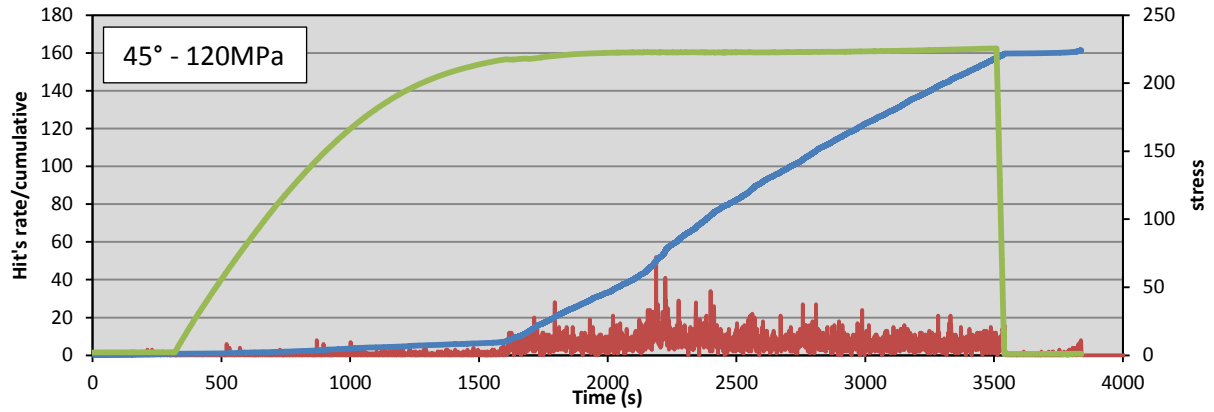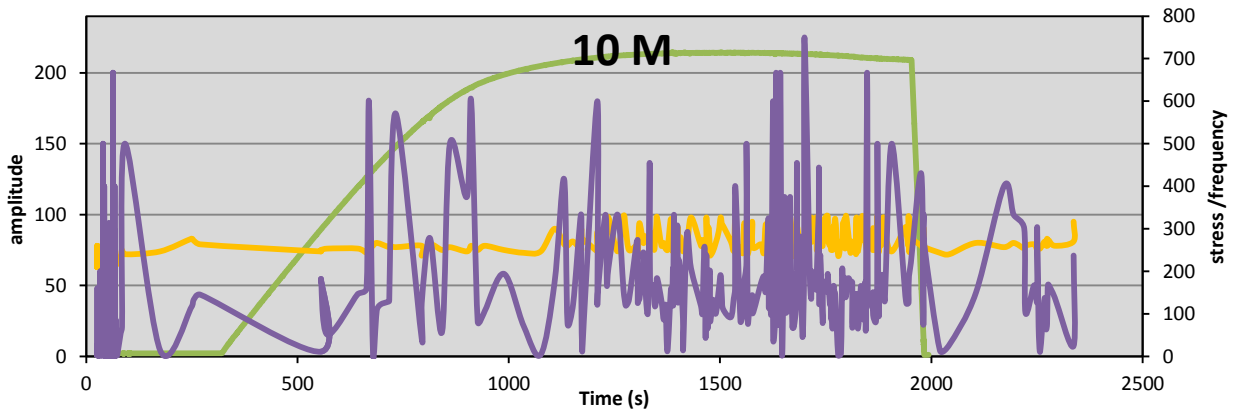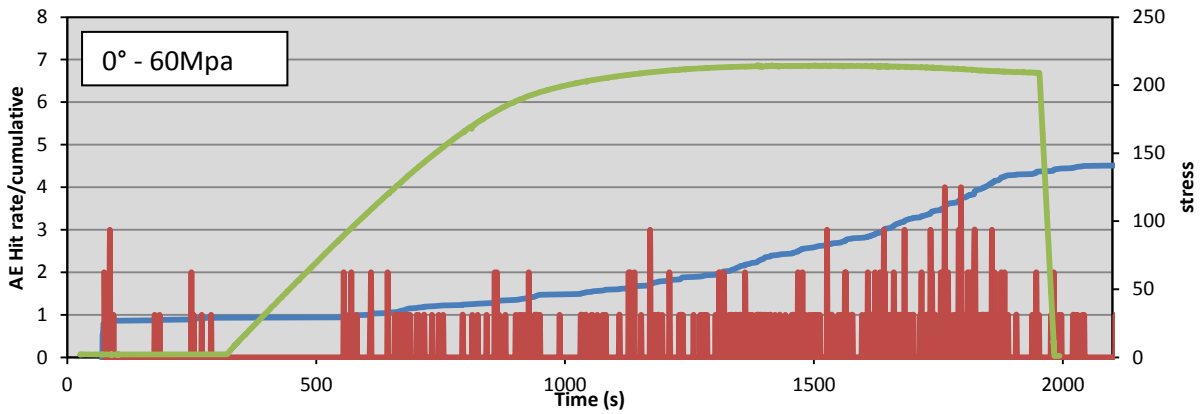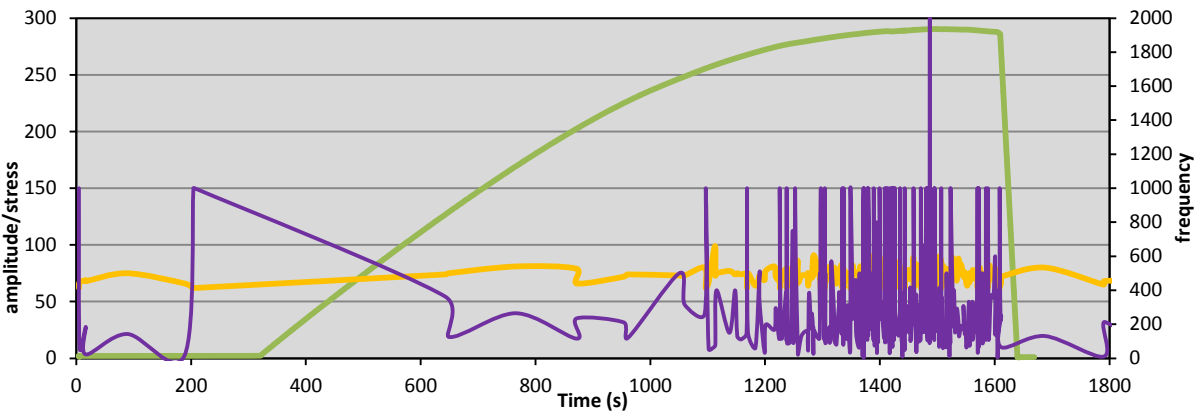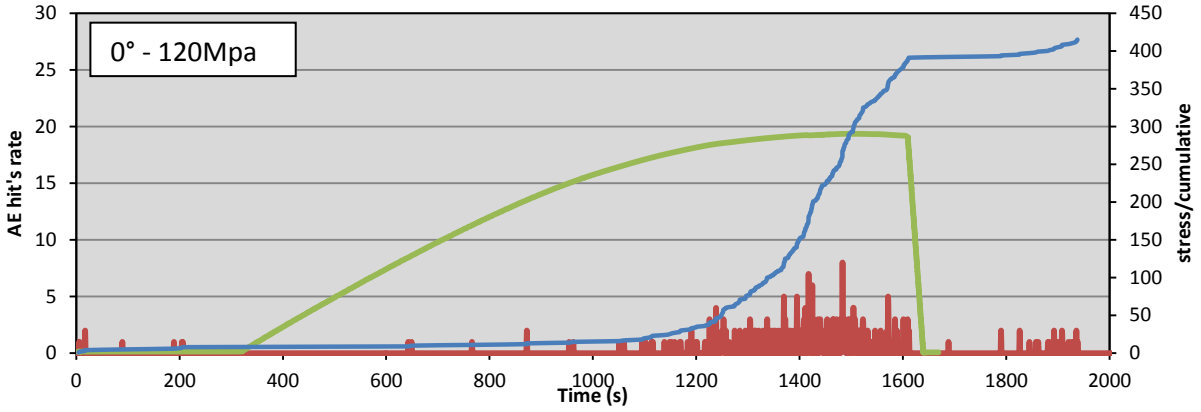
3.6 Referencies

ASTM Standard D4543-04, 2004. Standard Practices for Preparing Rock Core Specimens and Determining Dimensional and Shape Tolerances. ASTM International, West Conshohocken, PA (www.astm.org)

Attewell, P.B.&Sandford,M. R. 1974. Intrinsic shear strength of a brittle, anisotropic rock I: experimental and mechanical interpretation. International Journal of Rock Mechanics and Mining Science & Geomechanics Abstracts, 11, 423–430.

Bell, F.G. & Coulthard, J. M. 1997. A survey of some geotechnical properties of the Tees Laminated Clay of central Middlesbrough, North East England. Engineering Geology, 48, 117–133.

Bistacchi, A., Massironi, M., Menegon, L., Bolognesi, F., Donghi, V., 2012. On the nucleation of non-Andersonian faults along phyllosilicate-rich mylonite belts. Geol. Soc. London, Spec. Publ. 367, 185–199. doi:10.1144/SP367.13

Collettini, C., Niemeijer, A., Viti, C., Marone, C., 2009. Fault zone fabric and fault weakness. Nature 462, 907–10. doi:10.1038/nature08585

Donath, F. A. 1961. Experimental study of shear failure in anisotropic rocks. Geological Society of America Bulletin, 72, 985–990.

Donath, F. A. 1972. Effects of cohesion and granularity on deformational behavior of anisotropic rocks. Geological Society of America, Memoirs, 135, 95–128.

Duveau,G.,Shao, J.F.&Henry, J.P. 1998. Assessment of some failure criteria for strongly anisotropic materials. Mechanics of Cohesive-Frictional Materials, 3, 1–26.

Handy, M.R., 1990. The solid-state flow of polymineralic rocks. J. Geophys. Res. 95, 8647–8661.

Holdsworth, R.E., van Diggelen, E.W.E., Spiers, C.J., de Bresser, J.H.P., Walker, R.J., Bowen, L., 2011. Fault rocks from the SAFOD core samples: Implications for weakening at shallow depths along the San Andreas Fault, California. J. Struct. Geol. 33, 132–144. doi:10.1016/j.jsg.2010.11.010

Jaeger, J. C. 1960. Shear failure of anisotropic rocks. Geol. Mag. 97,65-72.

Jaeger, J.C., Cook, N.G.W., Zimmerman, R.W., 2007. Fundamentals of Rock Mechanics, 4th editio. ed. Wiley-Blackwell.

Kronenberg, A.K., Kirby, S.H., Pinkston, J., 1990. Basal slip and mechanical anisotropy of biotite. J. Geophys. Res. 95, 19257. doi:10.1029/JB095iB12p19257

McLamore, R. & Gray, K. E. 1967. The mechanical behavior of anisotropic sedimentary rocks. J. Engng Ind. 89, 62-76.

Richards, J. A. 1999. Remote Sensing Digital Image Q9 Analysis. Springer.

Rawling, G.C., 2002. Dilatancy, brittle strength, and anisotropy of foliated rocks: Experimental deformation and micromechanical modeling. J. Geophys. Res. 107, 2234. doi:10.1029/2001JB000472

Shea, W.T., Kronenberg, K., 1992. Rheology and Deformation Mechanisms of an Isotropic Mica Schist exponential constants O • ss MPa -1 and MPa -1 that account for the dif ; studies properties and 97.

Shea, W.T., Kronenberg, A.K., 1993. Strength and anisotropy of foliated rocks with varied mica contents 15.

Van Diggelen, E.W.E., De Bresser, J.H.P., Peach, C.J., Spiers, C.J., 2010. High shear strain behaviour of synthetic muscovite fault gouges under hydrothermal conditions. J. Struct. Geol. 32, 1685–1700. doi:10.1016/j.jsg.2009.08.020

Walsh, J. B. & Brace,W. F. 1964. A fracture criterion for brittle anisotropic rock. Journal of Geophysical Research, 69, 3449–3456.

4   Conclusions

The association between weak faults and phyllosilicates organized along regional-scale metamorphic mylonites is evidenced by many examples in continental deformation belts, both in collisional environments (e.g. Cox 1995; Collettini et al. 2009; Bistacchi et al. 2010), extensional environments and rifts (e.g. Wernicke 1981; Numelin et al. 2007; Smith & Faulkner 2010) and large-scale strikeslip or transform faults (e.g. Stewart et al. 2000; Holdsworth et al. 2011). Phyllosilicates, even in relatively small quantities, dramatically influence the mechanical behavior of rocks (e.g. Collettini et al., 2009; Van Diggelen et al., 2010; Holdsworth et al., 2011). In laboratory triaxial tests on foliated rocks, for a content in phyllosilicates greater than 20-25%, a relevant mechanical anisotropy appears, as the internal friction coefficient (tangential stress/normal stress at failure) varies between 0.3 and 0.7 with orientation of the sample with respect to the maximum compressive stress (Jaeger et al. 2007, Kronenberg et al. 1990; Moore & Lockner 2004, Bistacchi et al.2012). This reflects different fracture modes: when the foliation is favourably oriented, fractures develop along it and the rocks are weak, whilst when fractures cut the foliation at a high angle, rocks are stronger (Jaeger et al., 2007).

Field examples of misoriented faults represented by the Simplon Line Fault Zone (SFZ), in the Swiss Alps, and a zone of (ultra)cataclastic bands in the Grandes Rousses Massif of the French Alps (GRM). Their characterizations from the regional scale (paleostress), to the meso-scale (fault zone architecture), and micro-scale (optical microscope, SEM) highlight some analogies:

- misoriented fault planes nucleates along foliation planes where mica is concentrated
- cataclastic layers develop progressively thickening along foliation planes
- misoriented fault planes inhibit the Andersonian fracture development, which in mechanical terms means that the differential

Moreover, SL rocks are locally characterized by carbonate presence, recording fluid circulation: geometrical relationship between carbonates and hosting rock show how fluids exploite cataclastic layers permeability to circulate and to inject itself in the more competent rock portions. It means their contribution to weakening for overpressure is not the primary weakening mechanisme responsible of SL nucleation. GRM, on the French Alps, is characterized also by the presence of Andersonian conjugated fractures, but the two different behaviours

arise for two different angle foliation/σ1: around 60° for misoriented faults along foliation plane and 70° for Andersonian fractures. It defines an angle of about 65° for the transition from the isotropic Andersonian behaviour a weak anisotropic, with decreasing in internal friction coefficient from 0.7 to 0.22.

The mechanical characterization of GRM's samples with UCS and TXT highlights the relationships between elastic moduli, peak strength, and failure modes, as a function of the ß angle. Peak strength follows a continuously varying anisotropy model, since we observe a progressive and continuous strength decrease from ß = 0° to ß = 45°, and a similarly smooth and continuous increase up to ß = 90°. If we consider the different failure modes, we can see a progressive transition from an Andersonian behavior (ß = 0° or 90°), a hybrid failure mode dominated by stair-stepping fractures, and a failure mode dominated by slip along phyllosilicate films (20° < ß < 70°). Lab reconstructed structures show the same shape of the one observed in the field, and transition between the weak behaviour and the isotropic one similarly happens for ß~ 70°.

The anisotropic nucleation observed both in the field and in lab tested samples highlights the micromechanics of brittle failure, explains the effect of mica content on the brittle strength of foliated rocks and suggest how mica first brittle deformation may works as strong strain localization factor and eventually create a favourable environment for fluid circulation and relative weakening mechanisms.